JGR Oceans

RESEARCH ARTICLE
10.1029/2024JC021455

Mechanisms of Tropical Sea Surface Salinity Variations at Seasonal Timescales

Antoine Hochet[1], **Soumaïa Tajouri**[1], **Nicolas Kolodziejczyk**[1], **and William Llovel**[1]

[1]Laboratoire d'Océanographie Physique et Spatiale, University of Brest, CNRS, IRD, Ifremer, UBO, IUEM, Brest, France

Abstract Climate-coupled models typically overestimate the amplitude of the seasonal cycle of sea surface salinity (SSS) in the tropics. A better understanding of the mechanisms controlling the seasonal variance of SSS could provide directions for improving the representation of the SSS seasonal cycle amplitude in these models. In this work, we use a novel framework, based on seasonal salinity variance budget (SVB), which we apply to the Estimating the Circulation and Climate of the Ocean (ECCO) state estimate, to study the mechanisms controlling the variance of seasonal SSS in the tropical oceans. Our findings reveal that oceanic advection, vertical diffusion, and freshwater fluxes from rivers and precipitation all play an important role in controlling the amplitude of the seasonal cycle, but their impact varies regionally. The SVB framework effectively distinguishes between "source" (mechanisms that enhance variance) and "sinks" (mechanisms that dampen variance). We show that vertical diffusion acts as the primary sink across most regions, except for the eastern Arabian Sea where precipitation dominates as the main sink. In other regions of the tropical oceans, precipitation and river runoff act as sources of variance. The effect of the advective term on the SSS variance is shown to be mainly the sum of two terms—first, a term associated with the spatial redistribution of the variability by the eddy-parametrized oceanic circulation, and second, a term associated to a transfer of salinity variance between the time mean and seasonal circulations.

Plain Language Summary Seasonal variations of sea surface salinity in the tropics play an important role in controlling the upper ocean stratification and therefore air-sea interactions. However, most climate models overestimate the amplitude of the seasonal variation of SSS in the tropics. A better understanding of the mechanisms involved in controlling SSS amplitude would help to define directions for improving climate models by identifying the misrepresented processes. In this article, we use a novel diagnostic to understand the mechanisms controlling the amplitude of this seasonal cycle in the tropical oceans. Our results show that the seasonal cycle results from a subtle balance between different terms. In most regions, vertical mixing acts to damp the amplitude of the SSS seasonal cycle, while precipitation, river runoff, and oceanic advective terms act to sustain SSS seasonal cycle. We further show that mesoscale eddies play an important role in the oceanic advective term, suggesting that a correct representation of their effect is important to correctly simulate the SSS seasonal cycle.

Key Points:

- A variance budget is used to analyze the seasonal variations in sea surface salinity of the tropical oceans
- Precipitation is a source (acts to increase) for the variance except in the eastern Arabian Sea where it is a sink (acts to decrease)
- Parametrized eddy fluxes act as an important source and vertical diffusion is the main sink term almost everywhere

Correspondence to:
A. Hochet,
antoine.hochet@univ-brest.fr

Citation:
Hochet, A., Tajouri, S., Kolodziejczyk, N., & Llovel, W. (2025). Mechanisms of tropical sea surface salinity variations at seasonal timescales. *Journal of Geophysical Research: Oceans*, *130*, e2024JC021455. https://doi.org/10.1029/2024JC021455

Received 13 JUN 2024
Accepted 17 JAN 2025

Author Contributions:
Conceptualization: Antoine Hochet
Investigation: Antoine Hochet
Methodology: Antoine Hochet
Writing – original draft: Antoine Hochet
Writing – review & editing: Antoine Hochet, Soumaïa Tajouri, Nicolas Kolodziejczyk, William Llovel

1. Introduction

The most intense branch of the hydrological cycle of the planet are the evaporation (E) and precipitation (P) flux over the ocean (Schmitt, 1995). These surface freshwater fluxes leave a strong imprint on the ocean surface salinity leading to high salinity values in subtropical regions where evaporation dominates, and low salinity values in tropical and high latitudes' regions where precipitation and river runoff dominates. It is expected that under global warming, the water-holding capacity of the air (the saturation water vapor pressure) will increase and that regions of net precipitation will become wetter and regions of net evaporation will become dryer (Held & Soden, 2006). These trends in P and E fluxes over the oceans are however difficult to observe directly, and the last IPCC report (Gulev et al., 2021) assigned "low confidence" to the globally averaged trends in P-E over the 20^{th} century. To circumvent this problem, the possibility to use the sea surface salinity as a proxy for the intensity and change of the ocean hydrological cycle has therefore become an active subject of research (Terray et al., 2012; Yu, 2011; Yu et al., 2020). Unlike the P and E fluxes, long-term in situ observations of sea surface salinity from research vessels and voluntary observing ships are indeed available since the 1950s (Delcroix & Hénin, 1991). Moreover, since 2010, the European Space Agency's (ESA) Soil Moisture and Ocean Salinity (SMOS), the joint National Aeronautics and Space Administration's (NASA)/Argentinian Satélite de Aplicaciones Científicas (SAC)-D Aquarius, and the NASA Soil Moisture Active Passive (SMAP) satellites have

provided near-global observations of SSS (Reul et al., 2020). Long-term salinity observations suggest that SSS tends to increase in regions where it is high and decrease in regions where it is low (Boyer et al., 2005; Curry et al., 2003; Durack et al., 2012; Skliris et al., 2014), in agreement with an intensification of the hydrological cycle. However, SSS is not only controlled by the surface freshwater fluxes but also by the ocean's dynamics that play an essential role in maintaining the salinity distribution (Zika et al., 2015). Depending on whether the SSS is directly controlled by the surface freshwater fluxes or by ocean dynamics or by a combination of both, the use of the SSS as a direct proxy of the surface freshwater fluxes may be limited (Vinogradova & Ponte, 2013; Yu, 2011). A better understanding of the mechanisms controlling the variability in sea surface salinity would therefore help to determine the relationship between SSS variability and surface freshwater fluxes.

Climate models are our primary tools for understanding and projecting current and future climate. Therefore, it is important that they accurately represent the SSS variability, especially the seasonal cycle, which dominates the SSS variability. However, several studies have shown that significant biases exist between the observed SSS seasonal cycle and its representation in the CMIP5/CMIP6 climate models (Fathrio et al., 2017; Y. Liu et al., 2022). In particular, the magnitude of seasonal salinity variations is stronger in the models than in observations in the tropical regions (Y. Liu et al., 2022), suggesting that one or several processes are not well represented in these models. To understand the reasons for this overestimation in climate models, and ultimately to reduce this bias, we first need to better identify the processes that control the amplitude of the seasonal cycle in observations and state-of-the-art ocean numerical models. This comprehensive analysis will provide valuable insights into the specific elements that are inaccurately represented in current climate models, paving the way for targeted improvements and more accurate predictions.

In tropical regions, the pronounced SSS seasonal cycle is due to continental river runoff and intense precipitation associated with the presence of the Intertropical Convergence Zone (ITCZ) and South Pacific Convergence Zone (SPCZ) in the Pacific. The strong seasonal SSS variability has motivated ongoing research on their underlying mechanisms (Akhil et al., 2014; Camara et al., 2015; Da-Allada et al., 2015; Houndegnonto et al., 2021; Lee et al., 2019; Matias et al., 2024; Qu et al., 2011; Terray et al., 2012; Tzortzi et al., 2013; Yu, 2014). In the tropical Pacific, pronounced seasonal variations of SSS occur in the eastern regions and along the Central American coastline (Delcroix et al., 1996; Delcroix & Hénin, 1991; Guimbard et al., 2017; Yu, 2014). In the tropical Atlantic, seasonal variations in SSS are particularly strong in the western tropical North Atlantic and in the Gulf of Guinea due strong seasonal precipitation associated with large runoff of the Amazon and Congo rivers, respectively (Dessier & Donguy, 1994; Reverdin et al., 2007; Tzortzi et al., 2013). These SSS variations influence near-surface stratification and may, in turn, affect air-sea interactions through the formation of the barrier layer (Lukas & Lindstrom, 1991), which is thought to play an important role for the regional climate (Mignot et al., 2012). In the Indian Ocean, the greatest seasonal SSS amplitudes are observed in the northern Bay of Bengal and in the southeastern Arabian Sea (Rao & Sivakumar, 2003). The northern Indian Ocean is strongly influenced by the Indian monsoon, which causes winds to blow from the southwest in summer (May–September) and from the northeast in winter (November–March). This wind reversal induces a strong constraint on the upper ocean circulation (Shankar et al., 2002) and is accompanied by important changes in precipitation patterns, which in turn exert a strong influence on the SSS seasonal cycle. In addition, runoff from the Brahmaputra and Ganges rivers exert an important impact on the Bay of Bengal.

The main tool so far to understand the mechanisms of SSS seasonal variations has been the calculation of the different terms of the salinity budget in the mixed layer (e.g., Akhil et al., 2014; Camara et al., 2015; Da-Allada et al., 2013; Da-Allada et al., 2015; Lee et al., 2019; Yu, 2023). Seasonal salinity budgets are useful tools for understanding qualitatively the main mechanisms that control salinity time tendencies. However, this methodology has an important drawback in that it is difficult to obtain a quantitative assessment of the mechanisms as it is based on the visual inspection of the seasonal variations of the salinity tendencies and of the terms of its decomposition (i.e., advection, diffusion, and freshwater fluxes in its simplest form).

To circumvent this problem, some authors have computed the local correlation between the salinity time tendencies and the different terms from its decomposition (e.g., Yu, 2011). Although this methodology has the advantage of providing quantitative information, the resulting equation (i.e., $\left(\frac{\partial S'}{\partial t}\right)^2$ with S' the seasonal salinity anomaly) is hard to interpret in terms of physics.

In this study, we propose to use a new methodology, based on budget of salinity variance (BSV). This diagnostic has recently proven useful to study the mechanisms of interannual variability of salinity in the Arctic (Hochet, Lique, et al., 2024). A main advantage is that it allows to explicitly quantify the local mechanisms that act to increase (so called "sources") and decrease (so called "sinks") the amplitude of the seasonal SSS and provides a rigorous framework to physically interpret the different components of the oceanic advective term. Similar density variance budgets have been used in the literature to study the mechanisms of the Atlantic Multidecadal Variability (AMV) (Arzel et al., 2006, 2018; Buckley et al., 2012; Colin de Verdière & Huck, 1999; Gastineau et al., 2018; Hochet et al., 2015, 2022). It has also been applied to study the interaction between mesoscale turbulence and the AMV for the ocean temperature (Hochet et al., 2020), to study ENSO mechanisms (Boucharel et al., 2015; Guan & McPhaden, 2016; Guan et al., 2019; B. Liu et al., 2024) and the mechanisms of steric sea level interannual and seasonal variability (Hochet et al., 2023; Hochet, Llovel, et al., 2024). Additionally, tracer variance budget is widely used to study oceanic mixing (e.g., Gregg et al., 2018; MacCready et al., 2018; Osborn & Cox, 1972). Here, we derive a similar variance budget for the seasonal sea surface salinity and apply this budget to the Estimating the Circulation and Climate of the Ocean (ECCO) v4r4 state estimate (Forget et al., 2015).

This article is organized as follows: In Section 2, we describe the methodology of the SSS seasonal local variance budget, and in Section 3, we present the ECCO v4 state estimate used to compute this budget. Section 4.1 presents a comparative analysis of seasonal SSS variability between ECCO v4 and satellite observations, and Section 4.2 results from calculating the components of the seasonal SSS variance budget in ECCO v4. In Section 4.3, the time evolution of the corresponding terms in the SSS budget is discussed. In Section 4.4, we describe the decomposition of the advective term from the variance budget into several components corresponding to different physical mechanisms, and in Section 4.5, we provide the horizontal average of each term of the SSS seasonal variance budget over selected regions. Finally, we conclude and present the broader implications of our findings for future research in Section 5.

2. Method

2.1. Seasonal SSS Evolution Equation

Each variable X, obtained from the monthly averaged outputs of ECCO v4r4, is first decomposed into time mean and seasonal cycle as:

$$X = \overline{X} + X' + X^R \tag{1}$$

where $\overline{X}$ is the time mean (over the ECCO v4r4 period 1993–2016); X' the seasonal cycle anomaly is computed as the time mean of the monthly time series, that is,:

$$X'(m) = \frac{1}{N_{year}} \sum_{yr=1}^{N_{year}} X(m, yr) - \overline{X}, \tag{2}$$

where m and yr are the month and year indices, respectively, N_{year} is the number of years of the studied period (23 years for ECCO v4r4), and X is the monthly average output of ECCO v4. Note that we therefore have $\overline{X'} = 0$: the time mean of the seasonal cycle anomaly is zero. X^R in Equation 1 is the remaining salinity anomalies associated to interannual and subannual frequencies obtained as $X^R = X - \overline{X} - X'$. Applying Equation 2 to the evolution equation for the sea surface salinity gives an equation for the seasonal variations of the sea surface salinity anomaly S' as:

$$\frac{\partial S'}{\partial t} = \underbrace{-\nabla \cdot (\mathbf{V}S)'}_{=\text{adv}} + \underbrace{D_H' + D_V'}_{=\text{dif}} + \underbrace{(1/h(E - P - R)S)'}_{=\text{flu}} \tag{3}$$

where adv represents the advective terms with $\mathbf{V} = \mathbf{v} + \mathbf{v}_{GM}$ the residual velocity, that is, the sum of the resolved ($\mathbf{v}$) and parametrized velocities ($\mathbf{v}_{GM}$), here using the Gent and Mcwilliams (1990) scheme (GM hereafter), and dif all the horizontal (D_H') and vertical (D_V') diffusive terms associated with parametrized vertical mixing, diapycnal and isopycnal mixing, and flu; the effect of the surface freshwater fluxes associated with evaporation (E), precipitation (P), and river runoff (R). h represents the thickness of the first layer in ECCO v4.

2.2. Seasonal SSS Variance Budget

Because we want to understand the mechanisms that control the variance (i.e., amplitude) of the seasonal cycle, we derive an equation for the variance of the seasonal salinity cycle, that is, S' that we call the seasonal salinity variance budget (SVB). Using the decomposition of the sea surface salinity into its different components given by Equation 1, the time mean of the squared salinity can be decomposed as follows:

$$\overline{S^2} = \overline{S}^2 + \overline{S'^2} + \overline{S^{R2}}. \tag{4}$$

The first term on the right-hand side is the squared mean salinity; the second term is the seasonal variance, which is the main focus of this paper; and the last term is the variance of the remaining salinity anomalies S^R. The seasonal SVB is obtained by calculating the time average of the product between S' and Equation 3:

$$\overline{S'\frac{\partial S'}{\partial t}} = \overline{\frac{1}{2}\frac{\partial S'^2}{\partial t}} = \underbrace{\overline{S'\mathrm{adv}}}_{\mathrm{VAR_{adv}}} + \underbrace{\overline{S'\mathrm{dif}}}_{\mathrm{VAR_{dif}}} + \underbrace{\overline{S'\mathrm{flu}}}_{\mathrm{VAR_{flu}}}. \tag{5}$$

The left-hand side term represents the time mean of the variance time tendency and, the three terms on the right-hand side $\mathrm{VAR_{adv}}$, $\mathrm{VAR_{dif}}$, and $\mathrm{VAR_{flu}}$ are, respectively, the effect of oceanic advection, diffusion, and external freshwater fluxes. In this equation, if we find that one of the right-hand side terms is positive, it therefore contributes positively to the seasonal salinity variance in which case it is called *a source* because it acts to sustain the seasonal cycle. On the contrary, if we find that one of the right-hand side terms is negative, it acts to damp the seasonal salinity variance and it is called a *sink*.

Because of the methodology we use to extract the mean seasonal cycle anomaly (see Equation 2), the left-hand side in Equation 5 is not exactly zero: it represents the mean increase or decrease of the seasonal cycle amplitude over the period of interest (see also Appendix A). However, we will see in Section 4.2 that this term is much smaller than the right-hand side terms and can be neglected in the budget. The three terms from the right-hand side therefore approximately cancel. For example, if $\mathrm{VAR_{flu}}$ is locally positive, this means that it is a local source of SSS seasonal variance, and one of the two remaining terms (or the sum of the two) must be negative, and thus a sink, to compensate for the source, otherwise the amplitude of the variations would increase.

2.3. Decomposition of the Advective Term

Following a methodology similar to that used in Hochet et al. (2023), the advective term $\mathrm{VAR_{adv}}$ can be further decomposed into different terms arising from different dynamical features. For this purpose, the salinity advection term adv from Equation 3 is decomposed as follows:

$$\mathrm{adv} = -\nabla\cdot\left(\overline{\mathbf{V}}+\mathbf{V}'\right)S' - \nabla\cdot\mathbf{V}'\overline{S} + \nabla\cdot\left(\overline{\mathbf{V}'S'}\right)\underbrace{-\nabla\cdot\left(\mathbf{V}^R S^R\right)' - \nabla\cdot\mathbf{V}^R S' - \nabla\cdot\mathbf{V}' S^R}_{=\mathrm{adv_R}} \tag{6}$$

where $\overline{\mathbf{V}}$, $\mathbf{V}'$, and $\mathbf{V}^R$ are the decomposition of $\mathbf{V}$ following the formula in Equation 1. $\mathrm{adv_R}$ represents the remaining terms associated to correlations between submonthly velocities and submonthly salinity anomalies not resolved by the monthly outputs, as well as to subannual and interannual variations. The $\mathrm{adv_R}$ term is found to be much smaller than the first two terms and is therefore neglected in what follows. A decomposition of the advective term from the variance equation is then obtained by multiplying Equation 6 by S' and time-averaging:

$$\mathrm{VAR_{adv}} \approx \underbrace{\overline{-\nabla\cdot\left(\overline{\mathbf{V}}+\mathbf{V}'\right)\frac{S'^2}{2}}}_{=\mathrm{VAR_{adv}^{adv}}} \underbrace{-\overline{\mathbf{V}'S'}\cdot\nabla\overline{S}}_{\mathrm{VAR_{adv}^{mean}}} \tag{7}$$

The first term, $\mathrm{VAR_{adv}^{adv}}$ is interpreted as the seasonal SSS variance advection by the mean $\left(\overline{\mathbf{V}}\right)$ and seasonal residual velocities $(\mathbf{V}')$. This term represents the effect of the spatial redistribution of the seasonal salinity variance caused by the oceanic circulation and would sum to zero if we integrated it over the global ocean volume.

$\mathrm{VAR}^{\mathrm{adv}}_{\mathrm{adv}}$ acts as a source of seasonal SSS variance when there is a convergence of SSS variance fluxes (i.e., $\overline{\left(\overline{\mathbf{V}} + \mathbf{V}'\right)\frac{S'^2}{2}}$) and as a sink in the case of divergence. Although this term may be an important local source or sink of seasonal SSS variations, it cannot be responsible for the net creation or dissipation of variability globally. We call this term the advective spatially redistributing term.

The second term in Equation 7 (i.e., $\mathrm{VAR}^{\mathrm{mean}}_{\mathrm{adv}}$), unlike the first term, does not disappear when integrated over the global ocean volume (because it cannot be written as a divergence of a flux) and may act to decrease or increase the global salinity variance. This term is due to the residual salinity flux (i.e., $\overline{\mathbf{V}'S'}$) across the mean salinity surfaces (defined by $\overline{S} = \text{const.}$). $\mathrm{VAR}^{\mathrm{mean}}_{\mathrm{adv}}$ acts as a local source of salinity variance when the residual salinity flux is in the direction opposite to the mean salinity gradient $\left(\nabla\overline{S}\right)$ because, in this case, $-\overline{\mathbf{V}'S'} \cdot \nabla\overline{S} > 0$, and as a sink when it is in the direction of the mean salinity gradient (which implies that $-\overline{\mathbf{V}'S'} \cdot \nabla\overline{S} < 0$). It is straightforward to show that the same term but with an opposite sign appears in the equation for the squared time mean salinity (see also Hochet, Lique, et al., 2024).

$$\frac{1}{2}\frac{\partial\overline{S}^2}{\partial t} = -\frac{1}{2}\nabla\cdot\overline{\mathbf{V}}\,\overline{S}^2 - \overline{S}\nabla\cdot\overline{\mathbf{V}'S'} \tag{8}$$

$$= -\frac{1}{2}\nabla\cdot\overline{\mathbf{V}}\,\overline{S}^2 - \nabla\cdot\left(\overline{S}\,\overline{\mathbf{V}'S'}\right) + \underbrace{\overline{\mathbf{V}'S'}\cdot\nabla\overline{S}}_{=-\mathrm{VAR}^{\mathrm{mean}}_{\mathrm{adv}}}, \tag{9}$$

where we have only kept the advective terms and assumed that $S = \overline{S} + S'$ and $\mathbf{V} = \overline{\mathbf{V}} + \mathbf{V}'$ (i.e., the circulation is only made of the time mean circulation plus the seasonal cycle anomaly) to simplify the demonstration. The first two terms on the right-hand side of Equation 9 disappear when integrated over the ocean volume because they are written as the divergence of a flux, while the last term is the opposite of the term $\mathrm{VAR}^{\mathrm{mean}}_{\mathrm{adv}}$ from Equation 7. Hochet, Lique, et al. (2024) have therefore interpreted this term as a salinity variance transfer between the time mean salinity (more precisely, the $\frac{\overline{S}^2}{2}$ reservoir) and the variable salinity (here seasonal circulation, $\frac{\overline{(S')^2}}{2}$ reservoir). In other words, this term represents the interaction between the temporal mean salinity and the SSS seasonal cycle anomalies, reflecting their reciprocal influence: the seasonal cycle is partly shaped by the mean salinity and vice versa. In the remainder of this article, we will refer to $\mathrm{VAR}^{\mathrm{mean}}_{\mathrm{adv}}$ as the "salinity variance transfer term." An important novelty of this section is the decomposition of the oceanic advective term from the SSS variance equation into a first term associated with the spatial redistribution of the SSS variance and a second term associated with a SSS variance transfer between the time mean and the seasonal circulations.

2.4. Role of Eddy-Induced Transport

To understand the respective roles of the parameterized eddy-induced and resolved velocities, each term of the advection decomposition from Equation 7 can then be further decomposed into a part associated with the parameterization of the mesoscale eddies (GM bolus velocities) with an horizontal scale not resolved by the ECCO grid (111 km at low latitude) and a part associated with the resolved velocities:

$$\mathrm{VAR}^{\mathrm{X}}_{\mathrm{adv}} = \mathrm{VAR}^{\mathrm{X/GM}}_{\mathrm{adv}} + \mathrm{VAR}^{\mathrm{X/res}}_{\mathrm{adv}} \tag{10}$$

Here $X =$ mean or adv and $\mathrm{VAR}^{\mathrm{X/GM}}_{\mathrm{adv}}$, $\mathrm{VAR}^{\mathrm{X/res}}_{\mathrm{adv}}$ are, respectively, the part linked with the parametrized eddy-induced velocities and resolved velocities. These parameterized eddy-induced velocities reproduce the effect of baroclinic instability of the circulation, which act to flatten isopycnal surfaces by releasing potential energy (Gent & Mcwilliams, 1990).

3. The ECCO v4 State Estimate

To evaluate each term of the SSS variance budget, we use the ECCO v4r4 state estimate (Forget et al., 2015), which allows to close the salinity budget over the period 1993–2016. This state estimate is computed using the MITgcm and assimilates an ensemble of available observations using an adjoint method over the entire period of integration (Heimbach et al., 2005). The methodology used by the ECCO consortium implies that there are no

unphysical sources or sinks of salinity or heat, making it suitable for calculating physically sound tracer budgets. Among the salinity observations assimilated in ECCO v4r4 are in situ salinity from CTDs, moorings, Argo floats, gliders, and sea surface salinity from the Nasa Aquarius mission. ECCO v4 is forced using ERA-Interim atmospheric reanalysis fields (Forget et al., 2015) and a seasonal climatology of runoff from Fekete et al. (2002). The solution used in this article is computed on the LLC90 grid, which has a horizontal resolution ranging from 111 km in the tropics to 40 km at high latitudes and 50 vertical levels. Mesoscale turbulence is therefore not resolved and its effect is parameterized using GM. Additionally, it is worth noting that ECCO, unlike many other forced ocean simulations, does not have a surface salinity restoring term because the precipitation flux term is corrected using the adjoint method. In this work, each term is calculated from monthly averaged outputs, except the salinity time tendencies, which are obtained from snapshots at the beginning and end of each month. The seasonal cycle studied here is thus an average of the seasonal cycle over the 23 years of the 1993–2016 period. We focus on the tropical oceans, between 35°S and 35°N, which are characterized by their strong seasonal cycle in SSS.

4. Results

4.1. Comparison of ECCO v4 and the CCI SSS Data Sets

To assess the ECCO v4r4 state estimate, we use the climate change initiative (CCI) SSS data set. This data set is constructed from the merging of three satellite instruments: SMOS (Soil Moisture and Ocean Salinity), Aquarius, and SMAP (Soil Moisture Active Passive). The product used in this study (v04.41) is provided on a global grid with a spatial resolution of 25 km and a time resolution of 1 month (Boutin et al., 2021). The SSS variance obtained from the CCI SSS data set and the ECCO v4r4 data set show reasonable agreement (Figures 1a and 1b) with the largest values in the plume regions of the Amazon, Congo, and Brahmaputra River, as well as in the eastern Arabian Sea, Panama Bight, and southern Maritime Continent. Nevertheless, the observed SSS variance from the CCI data set is generally larger than that from the ECCO state estimate, particularly in the Amazon plume region where the large variability extends further north in the observations. The time-averaged SSS also shows similar patterns in the CCI and ECCO v4 data sets (Figures 1c and 1d). In the Pacific, both data sets agree on the location of mean SSS variations with freshwater to the east and along the equatorial band and salty water in the subtropics. In the Atlantic, both data sets show freshwater in the equatorial band and along the Amazon and Congo plume regions, and salty water in the northern and southern subtropical regions. In the Indian Ocean, both data sets agree on the presence of salty waters in the Arabian Sea and a decreasing mean SSS eastward as well as low mean SSS in the Maritime Continent. The eight regions with the highest levels of SSS variance, that is, the East Pacific region, the Panama Bight, the Amazon plume, the Congo plume, the eastern Arabian Sea, the southern equatorial Indian region, the Ganges-Brahmaputra River plume, and the southern Maritime Continent, are outlined by eight red boxes in Figure 1, and will receive special attention in this study.

4.2. Seasonal Amplitude of SSS Anomalies: The Role of Advection, Diffusion, and Freshwater Fluxes

The three terms of the right hand side of the SSS variance budget (Equation 5) associated with oceanic advection (VAR_{adv}), diffusion (VAR_{dif}), and freshwater fluxes (VAR_{flu}) are shown in Figure 2, panels B, C, and D, respectively. The sum of the three terms is negligible (Figure 2, panel A) as expected from Equation 5, which means that any source of variance must have a sink of opposite sign to compensate. Oceanic advection (Figure 2, panel B) acts as a source of SSS seasonal variance at all locations, with its highest values (about 3 $psu^2\ yr^{-1}$) in the Amazon and Brahmaputra plume regions. On the contrary, oceanic diffusion acts as a sink in most regions (Figure 2, panel C), with its highest values in the Amazon and Ganges-Brahmaputra plume regions as well as in East Pacific, Panama Bight, and South Maritime Continent regions. The important role of diffusion in the seasonal variations of SSS was already noted in the Atlantic by Camara et al. (2015) and in the Bay of Bengal by Akhil et al. (2014). Interestingly, we also find here that diffusion can act as a weak source of variance in some localized regions of the Indian Ocean, mostly along the west coast of India and the south-central region of the Bay of Bengal. The diffusive term is associated with the vertical part of the diffusive flux, its horizontal part being negligible (Figure 3, panels A and B). The term associated with the freshwater fluxes (evaporation, precipitation, and river runoff) is, in almost all locations, a source of seasonal SSS variance except in the eastern Arabian Sea and, to a smaller extent, in the southern Bay of Bengal where it acts as a sink (Figure 2, panel D). To the best of our knowledge, this is the first time that freshwater fluxes are shown to dampen the amplitude of the SSS seasonal

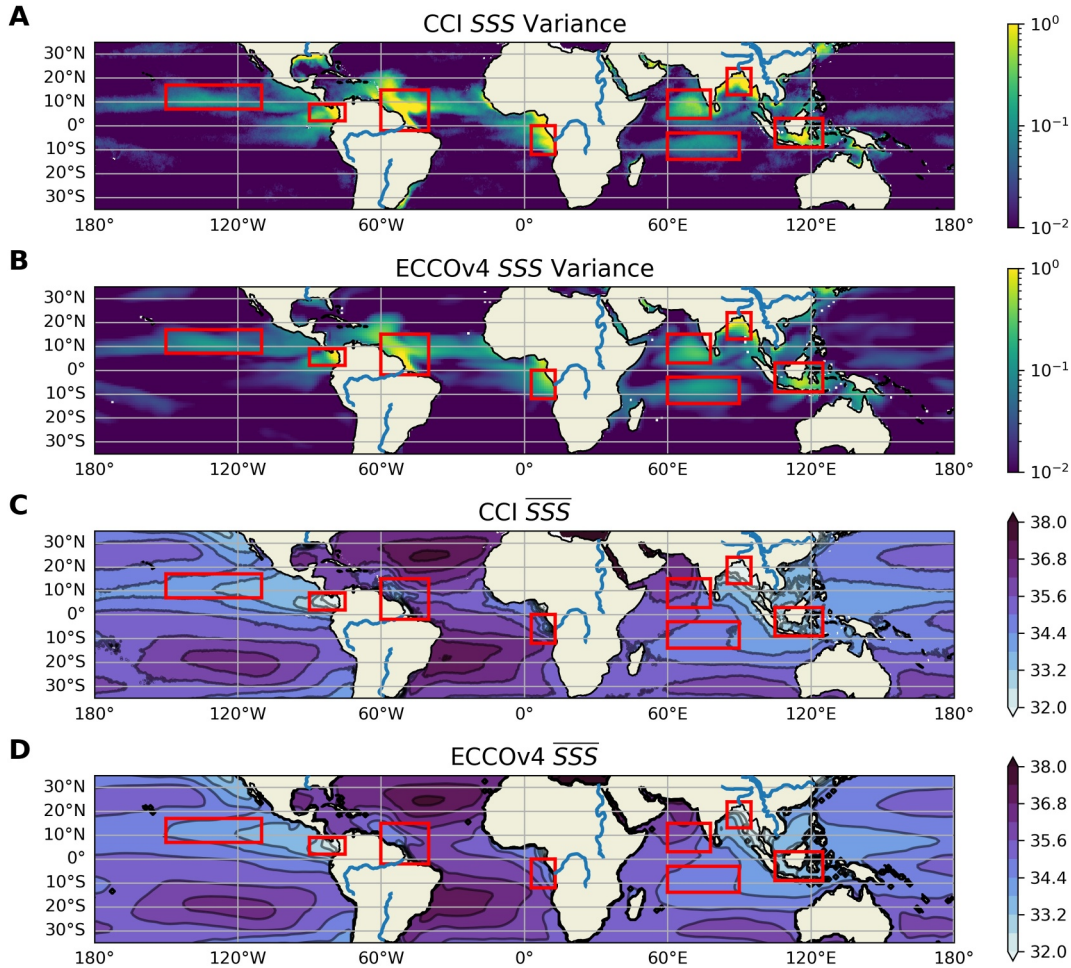

Figure 1. Comparison between the ECCO v4 ocean state estimate and the CCI SSS product. Panels a and b show, respectively, the SSS seasonal variance for the period 2010–2015 (5 years) for CCI and ECCO v4 (in psu^2). Panels c (CCI) and d (ECCO v4) show the time mean SSS (in psu) over 2010–2015. The eight red boxes outline eight regions characterized by their strong level of SSS seasonal variability: the East Pacific region, the Panama Bight, the Amazon plume region, the Congo plume region, the Eastern Arabian Sea, the southern equatorial Indian region, the Brahmaputra River plume, and the southern Maritime Continent.

cycle in these regions. Figure 3 shows that in some regions, the three right-hand side terms of the variance budget are important, for example, in the Amazon plume or in the southern Maritime Continent region, while in others, only two terms account for the main balance (namely diffusive and freshwater fluxes terms), for example, in the East Pacific region and in the southern equatorial Indian region. In the Mississippi plume region, the main balance appears to be between the advective term (a source) and the diffusive term (a sink). In the Amazon plume region, the amplitude of the terms shown in panels B, C, and D (Figure 2) is of 3 $psu^2\ yr^{-1}$, while the SSS variance amplitude in the same region is of 1 psu^2 (Figure 1b). Therefore, if there were no source to compensate for the sink effect of the diffusive term in this region, these amplitudes suggest that a timescale of about 4 months (1 psu^2/ 3 $psu^2\ yr^{-1}$) would be sufficient to completely dampen the SSS seasonal cycle.

To further understand the role of the different components of the freshwater flux term (panel D, Figure 2), we now decompose it into three different terms as follows:

$$\mathrm{VAR}_{\mathrm{flu}} = \mathrm{VAR}_{\mathrm{flu}}^{\mathrm{roff}} + \mathrm{VAR}_{\mathrm{flu}}^{\mathrm{precip}} + \mathrm{VAR}_{\mathrm{flu}}^{\mathrm{evap}} \tag{11}$$

where $\mathrm{VAR}_{\mathrm{flu}}^{\mathrm{roff}}$, $\mathrm{VAR}_{\mathrm{flu}}^{\mathrm{precip}}$, and $\mathrm{VAR}_{\mathrm{flu}}^{\mathrm{evap}}$ are ,respectively, the terms associated to river runoff, precipitation, and evaporation. The dominant term from this decomposition is the one associated with precipitation (Figure 3c),

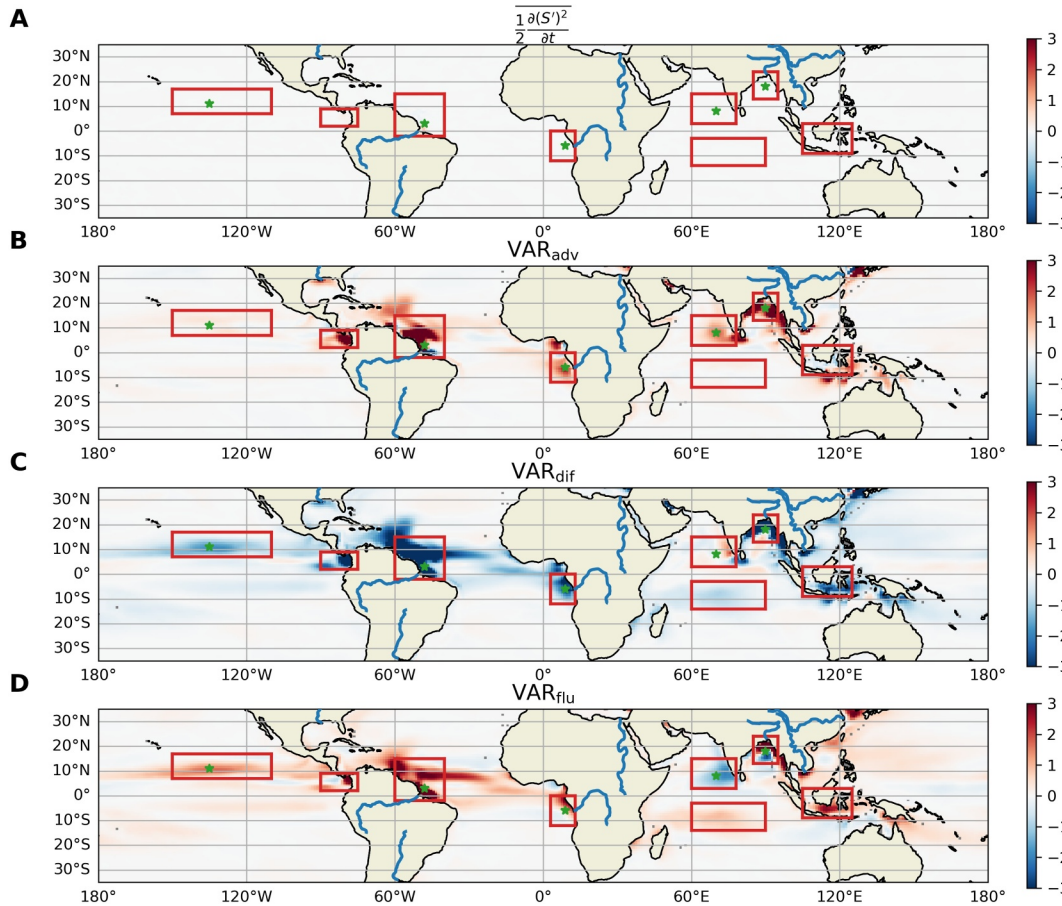

Figure 2. Seasonal SSS variance budget in ECCO v4 ($psu^2\ yr^{-1}$) (1993–2016). Panel a: SSS variance tendency $\overline{\frac{1}{2}\frac{\partial (S')^2}{\partial t}}$. Panel b: Term associated with oceanic advection. Panel c: Term associated with the diffusion. Panel d: Term associated with the surface freshwater fluxes (E–P) and river runoff. Green stars indicate the location where the SSS budget is analyzed in Section 4.3.

which is generally a source of SSS variance but also accounts for the sink pattern of the freshwater flux term in the eastern Arabian Sea. In this region, therefore, the seasonal precipitation anomaly is positive when the seasonal SSS anomaly is positive (i.e., it rains when the SSS is saltier), while the opposite is true in most other locations. In the western part of the eastern Arabian Sea region, the main source is associated with advection, balanced by the effect of precipitation, while in the eastern part, along the west coast of India, vertical diffusion is the main source, still balanced by the effect of precipitation. The important effect of vertical diffusion found along the west coast of India is coherent with Akhil et al. (2023)'s results. The river runoff term (Figure 3d) is only important near river mouths, and depends on its numerical parameterization in ECCO v4. It is an important source of SSS variability in the Amazon and Ganges-Brahmaputra River plume regions, but is only a weak source of variability in the Congo River plume region. Note that this term represents the direct effect of river runoff on SSS variability; rivers also affect SSS indirectly through advection. The term associated with evaporation (Figure 3e) is always smaller than the other two terms of the freshwater term decomposition and can be neglected in the budget. These results can be partly explained by the fact that the seasonal variations of the evaporation have a much smaller amplitude than those of the precipitation.

4.3. Seasonal Evolution of the SSS Budget and Link With the SSS Variance Budget

In this subsection, we seek to improve our understanding of the SSS variance budget by discussing the time evolution of the seasonal SSS budget Equation 3 at five locations, selected for their high level of variability: the East Pacific, the Amazon plume, the Congo plume, the Ganges-Brahmaputra plume, and the eastern Arabian Sea.

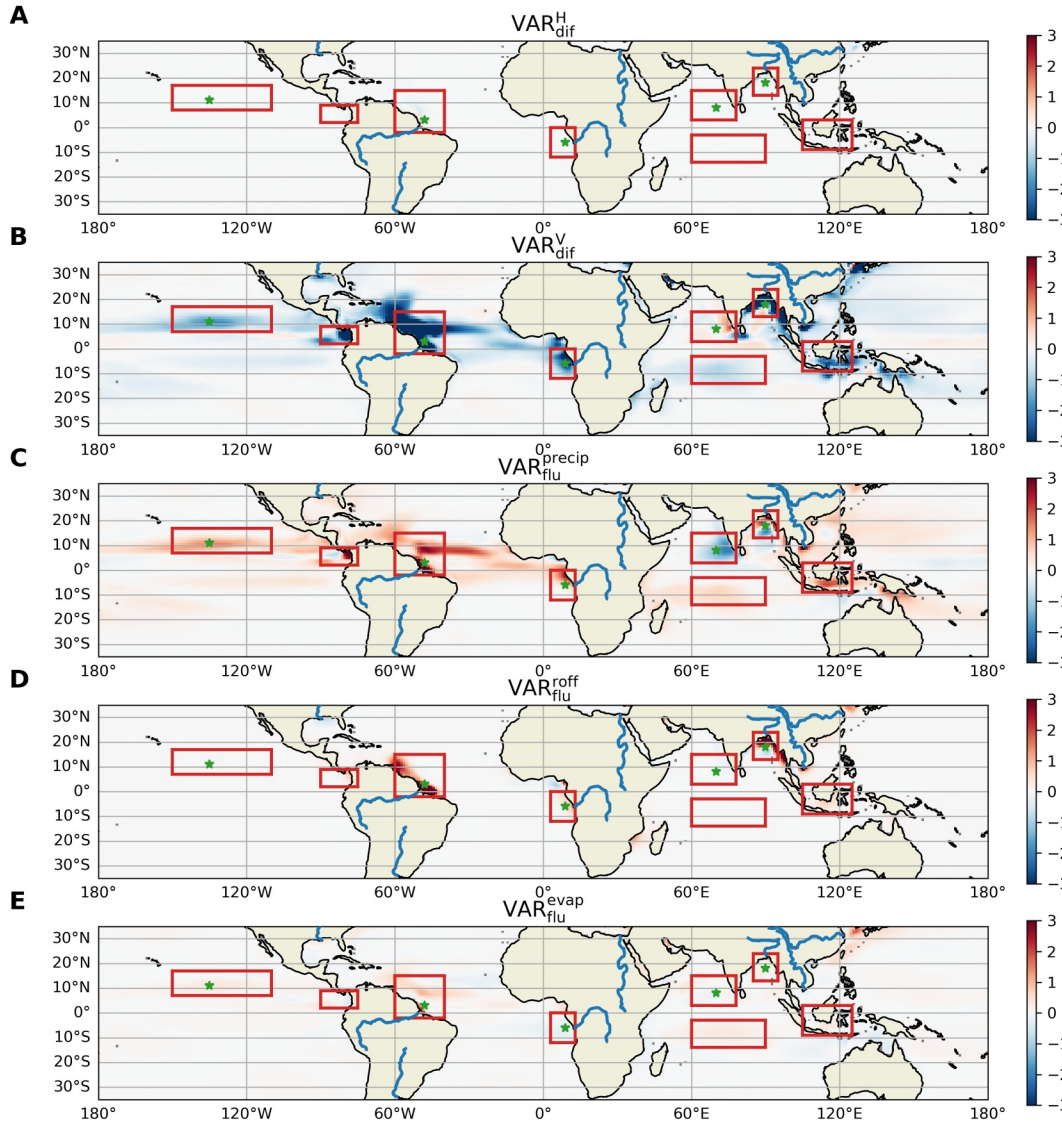

Figure 3. Panels a and b: Decomposition of the diffusive term from the seasonal SSS variance equation (VAR_{dif}, Figure 2, panel c) into horizontal diffusion VAR^{H}_{dif} (panel a) and vertical diffusion VAR^{V}_{dif} (panel b). Panels c–e: Decomposition of the freshwater flux term (Figure 2, panel d) into precipitation (panel c), river runoff (panel d), and evaporation (panel e). Units: $psu^2\ yr^{-1}$.

To be consistent with our local analysis, we choose to show the budget at local sites rather than using horizontal average across regions that would instead represent the dynamics at the horizontal scale of the region. The results shown in this section therefore partly depend on the location of the chosen site; however, each location within each region has been carefully selected to be consistent with the horizontal average of the SSS variance budget that will be presented in Section 4.5.

The first column of Figure 4 (panels A, D, G, J, and M) shows the time evolution of the different terms of the salinity budget from Equation 3 at the five selected locations. As expected, the time evolution of the salinity time tendency (blue line), that is, $\frac{\partial S'}{\partial t}$ is in quadrature with that of the salinity (dashed black line) in every region (see also Figure 2, panel A). In the salinity variance budget, a term is a source, that is, it acts to increase the amplitude of the SSS variations, if its time correlation with the salinity anomalies is positive, and conversely, it is a sink if this correlation is negative. The time evolution of the products of the salinity anomaly S' and of each term from Equation 3 are shown in the second column of Figure 4 (panels B, E, H, K, and N) and their time mean in the last column (panels C, F, I, L, and O). As explained in Section 2, this methodology differs from what is usually found

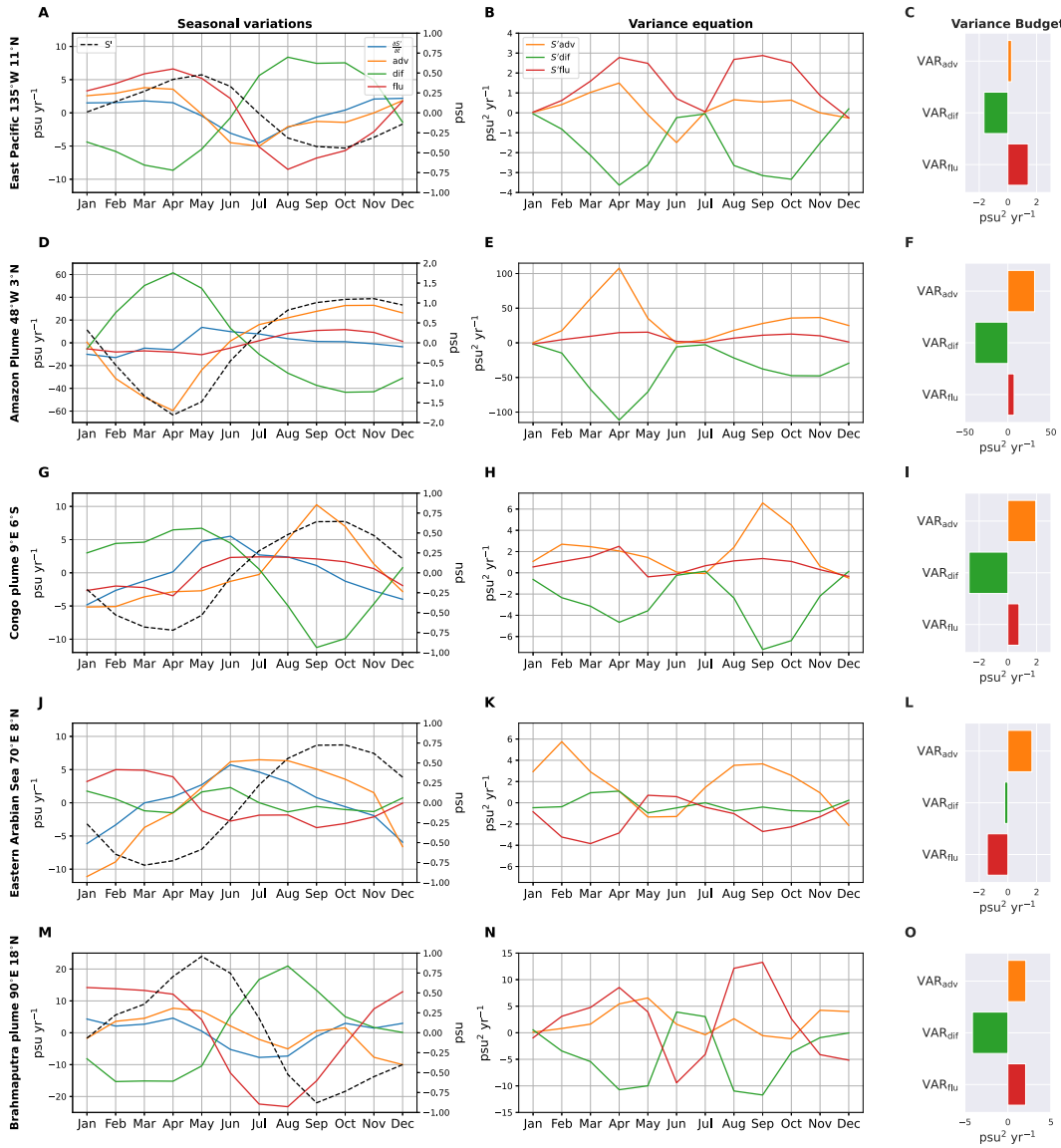

Figure 4. Monthly evolution of the seasonal SSS budget terms and corresponding salinity variance budget terms at five selected locations: the East Pacific (first row, panels a–c), the Amazon plume (second row, panels d–f), the Congo plume (third row, panels g–i), the eastern Arabian Sea (fourth row, panels j–l), and the Brahmaputra River plume (last row, panels m–o) (see also the green stars in Figures 2, 3). The first column (a, d, g, j, and m) shows the seasonal variations of each term of the seasonal SSS budget at each location: the time tendency $\frac{\partial S'}{\partial t}$ (blue), the advection adv (orange), the diffusion dif (green), and the freshwater fluxes flu (red). The black-dashed line represents the horizontally averaged SSS seasonal anomaly. Units are in psu yr^{-1} for the salinity budget terms and psu for S'. The second column (b, e, h, k, and n) shows the seasonal evolution of salinity variance budget terms computed as the product of S' with the right-hand side of the seasonal SSS budget: the advection term (orange line), the diffusion term (green line), and the surface freshwater flux term (red line) (units: $psu^2\ yr^{-1}$). The last column (c, f, i, l, and o) gives the seasonal variance budget (i.e., time mean of the second column) for advection (VAR_{adv}, orange), diffusion (VAR_{dif}, green), and surface freshwater fluxes (VAR_{flu}, red) (units: $psu^2\ yr^{-1}$).

in the literature, where most authors look at the main contributors to $\frac{\partial S'}{\partial t}$ (e.g., Akhil et al., 2014; Da-Allada et al., 2015), sometimes directly by calculating the correlation between the right-hand terms of Equation 3 and $\frac{\partial S'}{\partial t}$ (e.g., Yu, 2011). The terms that best correlate with $\frac{\partial S'}{\partial t}$ are generally not the same as those that correlate with SSS (because S' and $\frac{\partial S'}{\partial t}$ are in quadrature); thus, the mechanisms that control the salinity variance (i.e., amplitude) are expected to be different from the terms that best correlate with $\frac{\partial S'}{\partial t}$. Below is a detailed description of the salinity budget variations and the corresponding salinity variance budget at the five selected sites.

4.3.1. The East Pacific Site (135°W 11°N)

At the site in the East Pacific, the salinity anomaly is positive from January to June and negative from July to December (dashed black line Figure 4, panel A). Advection (orange line) is in phase with $\frac{\partial S'}{\partial t}$ (blue line) and of similar amplitude while both diffusion (green line) and freshwater (red line) have larger amplitudes than advection and are not in phase with $\frac{\partial S'}{\partial t}$. Therefore, the largest correlation is between $\frac{\partial S'}{\partial t}$ and the advection in agreement with previous studies (e.g., Yu, 2023). But, as mentioned above, the purpose of our study is to find the terms that contribute to maintaining (i.e., sources) and damping (i.e., sinks) the seasonal cycle, and this is obtained by computing the product between S' and the three right-hand side terms. This product is shown on panel B and reveals that the largest amplitudes are obtained for S'adv, which is always positive and for S'dif, which is almost always positive. S'adv has a smaller amplitude than the previous two terms and is negative in June and positive the rest of the year. The time average of the products (panel C) shows that the main balance is between a source associated with the freshwater fluxes 1.5 psu^2 yr^{-1} and a sink associated with diffusion −1.7 psu^2 yr^{-1}. Advection is a small source of seasonal salinity variance contributing to 0.2 psu^2 yr^{-1}. To better understand the respective roles of the three contributors to the freshwater flux term (i.e., precipitation, evaporation, and river runoff), we also show the monthly evolution of these three terms (Figure 5). The largest contribution to the freshwater flux term is due to the precipitation term 1.2 psu^2 yr^{-1}, while evaporation is a weak source of variance, contributing 0.3 psu^2 yr^{-1}.

4.3.2. The Amazon Plume Site (48°W 3°N)

At the site in the Amazon plume, the salinity anomaly is positive from July to January and negative from February to June (dashed black line Figure 4, panel D) with an amplitude around 1.5 psu. None of the three right-hand side terms in Equation 3 has negligible amplitude. The anomaly of the diffusive term (green line) has a sign opposite to that of the salinity anomaly; their product is thus negative (panel E) and contributes to decrease the SSS seasonal cycle amplitude (i.e., a sink) at a rate of −38 psu^2 yr^{-1} (panel F). On the contrary, the advective term anomaly (orange term) has only a small time lag with the salinity anomaly (approximately 1 month). Thus, their product is positive (panel E) and contributes to increase the SSS seasonal cycle amplitude, at a rate of 31 psu^2 yr^{-1} (panel F). The anomaly of the freshwater term has a smaller amplitude than the two other terms and is in phase with the salinity anomalies. It also contributes to increase the SSS seasonal cycle amplitude but at a lower rate than the advection term anomaly (7 psu^2 yr^{-1}). The amplitude of the evaporation term is small, so it can be neglected (Figure 5d), while the precipitation and runoff terms display greater amplitudes and are both in phase with the SSS anomalies. They both contribute to increase the SSS seasonal cycle variance at this location (Figures 5d–5f).

4.3.3. The Congo Plume Site (9°E, 6°S)

Except for an amplitude nearly 6 times smaller, the monthly variations of the seasonal SSS budget at the selected location in the Congo plume region are similar to those found at the Amazon plume site. The diffusive flux is opposite to the salinity variations and thus acts to reduce their amplitude, at a rate of −2.7 psu^2 yr^{-1} (Figures 4g–4i). On the contrary, the advection and freshwater flux terms act to increase it at a rate of 2 and 0.7 psu^2 yr^{-1}, respectively (panel I). It is worth noting that at this site, the evaporation term is nonnegligible and opposite to the salinity variations, thus acting as a sink of the SSS seasonal variance (−0.2 psu^2 yr^{-1}), opposing the effect of precipitation (0.6 psu^2 yr^{-1}) and river runoff (0.3 psu^2 yr^{-1}), which are both in phase with the salinity variations (Figures 5g–5i). In agreement with our results using seasonal salinity variance budget, Da-Allada et al. (2014) found that on seasonal timescales, freshening from horizontal advection and freshwater fluxes balances the salinization effects of vertical diffusion and vertical advection.

4.3.4. The East Arabian Sea Site (70°E, 8°N)

Compared to the two previous sites (i.e., Amazon and Congo), the seasonal SSS budget at the east Arabian Sea site is significantly different (Figure 4j). The amplitude of the diffusive term is smaller than the other terms of the budget (about 1 psu yr^{-1}). It has a semiannual timescale, and its correlation with the salinity anomaly leads to a weak decrease in the SSS seasonal cycle amplitude of −0.2 psu^2 yr^{-1} (panel J). We find a good correspondence between the advective term (orange line) and the SSS tendency term (i.e., $\frac{\partial S'}{\partial t}$, blue line), which is in agreement with results from previous studies (Da-Allada et al., 2015). On seasonal timescales, this region is strongly

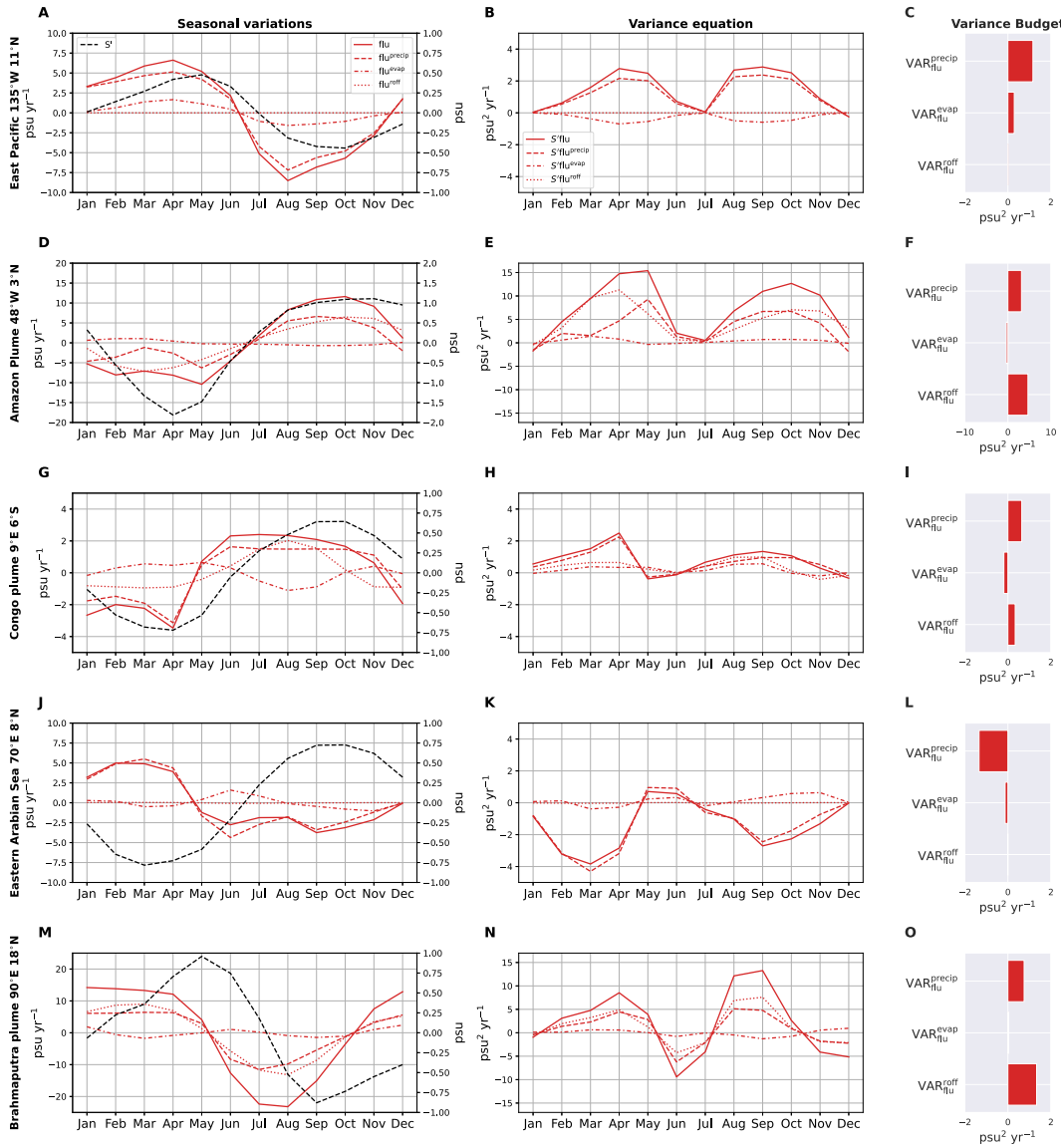

Figure 5. Same as Figure 4 except that the red lines represent the seasonal evolution of the freshwater flux term (solid red) and its decomposition into three terms relates to precipitation (dashed), evaporation (dashed dotted), and river runoff (dotted) (first column panels a, d, g, j, and m). The second column (panels b, e, h, k, and n) shows the product between the seasonal SSS anomaly and the freshwater flux term and its decomposition. The last column (panels c, f, i, l, and o) shows the contribution of the precipitation $\left(\mathrm{VAR}_{\mathrm{flu}}^{\mathrm{precip}}\right)$, evaporation $\left(\mathrm{VAR}_{\mathrm{flu}}^{\mathrm{evap}}\right)$ and river runoff $\left(\mathrm{VAR}_{\mathrm{flu}}^{\mathrm{roff}}\right)$ to the salinity variance budget.

influenced by the Indian monsoon, which leads to reversing winds north of 10°S, forcing strong seasonal variations in ocean circulation (e.g., Shankar et al., 2002). In the seasonal salinity variance budget at this site, advection contributes to increasing the amplitude of the variations (panel K) at a mean rate of 1.7 $\mathrm{psu}^2\ \mathrm{yr}^{-1}$ (panel L). Because the diffusion effect is small in this region, the advection effect must be balanced by another term. We find that this balance is accomplished by the effect of freshwater flux anomalies, which are generally positive (negative) when the salinity anomaly is negative (positive) thus leading to overall negative values (panel K) and a mean rate of salinity variance decrease of $-1.4\ \mathrm{psu}^2\ \mathrm{yr}^{-1}$. The freshwater flux term is almost entirely due to the seasonal cycle in precipitations (Figures 5j–5l). This precipitation term is an important component of the budget in this region because it acts to counteract the effect of advection. Without this term (all other things remaining equal), the variance would increase at a rate of 1.4 $\mathrm{psu}^2\ \mathrm{yr}^{-1}$.

4.3.5. The Ganges-Brahmaputra Plume Site (90°E, 18°N)

The selected site in the Ganges-Brahmaputra plume region has positive SSS anomalies from February to July and negative SSS anomalies from August to January (Figure 4m). The most striking feature is that the seasonal variation of the diffusion term seems to be opposite to that of the freshwater flux term (except for November and December). However, even though these two terms appear to be almost symmetric when looking at Figures 4m and 4n, the salinity variance budget shows that the contribution of the diffusive term is -4.1 psu^2 yr^{-1}, while that of the freshwater flux term is 2.1 psu^2 yr^{-1} (Figure 4o). Therefore, the contribution of these two terms to the salinity variance budget is not exactly balanced, and the advection term plays an important role (2 psu^2 yr^{-1}). The vertical diffusion anomaly is maximum in August and acts in the direction of a salinity increase. Thakur et al. (2019) has shown that, in this region, the intensity of the mixing in the upper 25 m of the water column is controlled by the wind forcing, which is maximum during the summer monsoon in June–September. Figures 5m and 5n show that evaporation is negligible at this site and that precipitation and river runoff appear to contribute almost equally as their seasonal evolution is quite similar. However, when we calculate the salinity variance budget (Figure 5o), we find that precipitation and river runoff account for 0.8 and 1.3 psu^2 yr^{-1}, respectively, showing that the effect of river runoff variability dominates.

4.4. Insights Into the Role of Oceanic Advection in Local SSS Anomalies Variations

In this subsection, the advective term (Figure 2b) is decomposed into two different terms following Equation 7 in order to understand the respective roles of the spatial redistribution of SSS variance and of the transfer of seasonal SSS variance.

4.4.1. The Salinity Variance Transfer Term

The seasonal salinity variance transfer term, associated with the salinity flux $\left(\overline{\mathbf{V}'S'}\right)$ in the direction of the mean salinity gradient $\left(\nabla\overline{S}\right)$, is a source of seasonal SSS variance at almost all locations and is enhanced in the river plumes as well as in the eastern Arabian Sea (Figure 6a). Using the decomposition into GM and resolved velocities given by Equation 10, we find that the salinity variance transfer term is associated with the resolved salinity flux (Figure 6e) while the parameterized salinity flux (Figure 6c) is less important overall although not negligible in certain regions such as the Panama Bight and the Mississippi River plume where it accounts for most of $\mathrm{VAR}_{\mathrm{adv}}^{\mathrm{mean}}$. $\mathrm{VAR}_{\mathrm{adv}}^{\mathrm{mean/res}}$ is mainly due to its horizontal component and thus to the resolved horizontal salinity flux $(\overline{\mathbf{v}_h S'})$ in the direction of the horizontal mean salinity gradient $\left(\nabla_h\overline{S}\right)$ (Figures 7a and 7b).

In the eastern Arabian Sea, where the advective term was found to be the main source of seasonal SSS variance in Figure 2b, the salinity variance transfer term associated with the resolved salinity flux through the mean salinity surfaces is the dominant source of seasonal SSS (Figure 6e). The latter term compensates for the sink associated with precipitations (Figure 2d). In the eastern Arabian Sea, the horizontal mean salinity gradient is toward the northwest (Figures 1c and 1d). To be positive and thus a source of seasonal SSS variance in this region, the resolved horizontal salt flux must be downgradient, that is, southeastward. Similarly, in other regions where $\mathrm{VAR}_{\mathrm{adv}}^{\mathrm{mean/res}}$ is a source of seasonal SSS variance, such as the Amazon plume region and the Gulf of Guinea, the resolved horizontal salt flux is also downgradient, that is, toward the Amazon river mouth in the Amazon plume region and toward the northeast in the Gulf of Guinea (Figures 1c, and 1d).

4.4.2. The Advective Spatially Redistributing Term

The spatially redistributing term, associated with the redistribution of seasonal SSS variance ($\mathrm{VAR}_{\mathrm{adv}}^{\mathrm{adv}}$ Figure 6b) is a source in most regions and has large positive values in the Panama Bight, Amazon, Congo, and Brahmaputra plume regions. As before, to better understand the physical processes that govern this term, we decompose it into a component due to the parameterized eddy velocity $\mathrm{VAR}_{\mathrm{adv}}^{\mathrm{adv/GM}}$ and a component associated with the resolved velocities $\mathrm{VAR}_{\mathrm{adv}}^{\mathrm{adv/res}}$ following Equation 10. The largest component is associated with the parameterized eddy velocity at almost all locations (Figure 6d). $\mathrm{VAR}_{\mathrm{adv}}^{\mathrm{adv/GM}}$ is positive almost everywhere indicating that it is a source of seasonal SSS variance. This result outlines the important role of (parameterized) mesoscale eddies in the redistribution of the seasonal SSS variance. The horizontal and vertical components of this term are important (Figures 7c and 7d) and are in close balance. It can further be shown that $\mathrm{VAR}_{\mathrm{adv}}^{\mathrm{adv/GM}}$ is almost entirely due to the

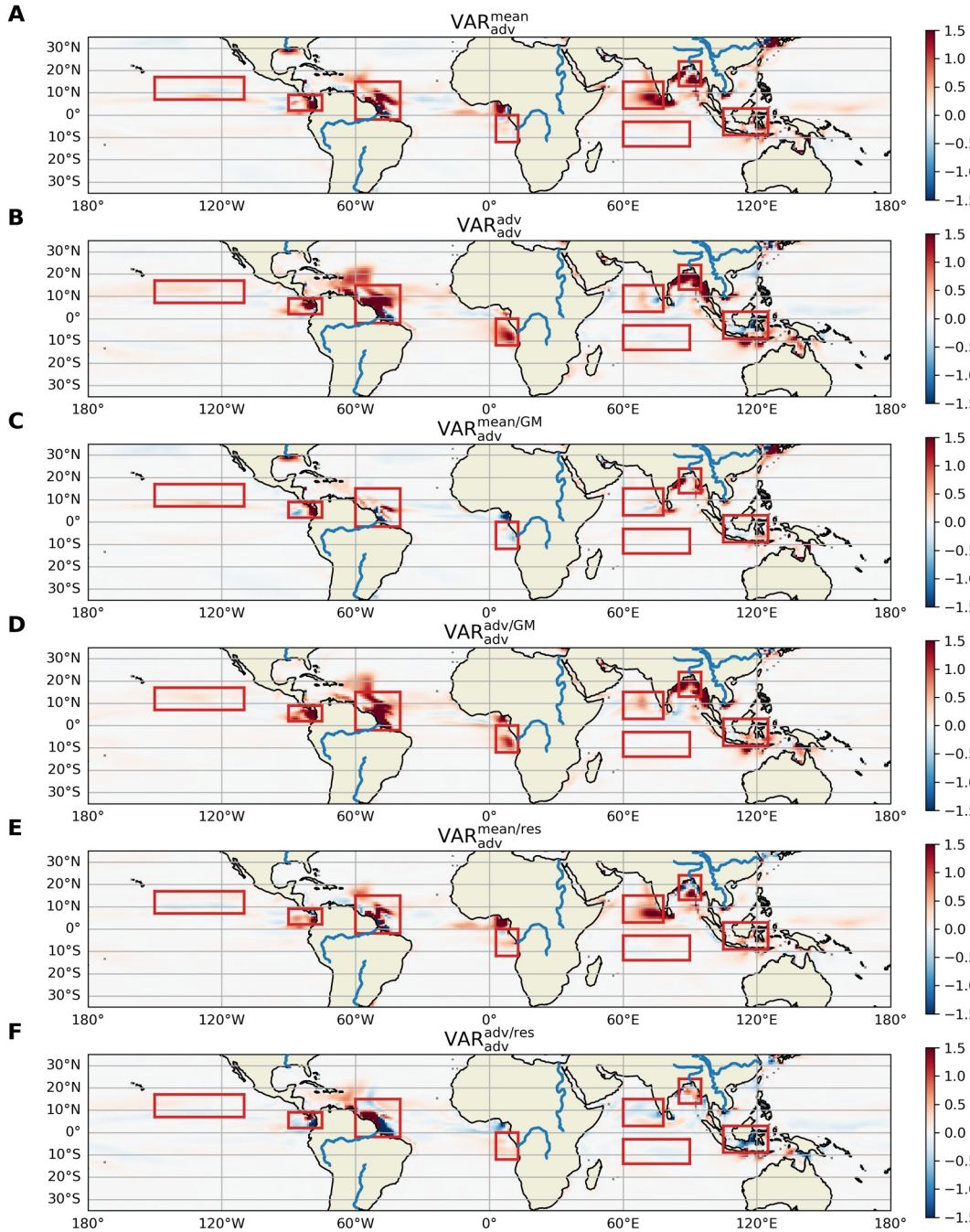

Figure 6. Decomposition of the advective term in the seasonal SSS variance budget ECCO v4 (psu^2 yr^{-1}) (1993–2016). Panel a: Term associated with the salinity flux across mean salinity surfaces due to the anomalous residual velocities $\left(-\overline{\mathbf{V}'S'}\cdot\nabla\overline{S}\right)$. Panel b: Term associated with the redistribution of seasonal SSS variance by the residual velocities $\left(-\nabla\cdot\overline{\left(\overline{\mathbf{V}}+\mathbf{V}'\right)\frac{S'^2}{2}}\right)$. Panels (c, e): Decomposition of the salinity variance transfer term (panel a) into a part associated with the GM-parametrized eddy velocity (panel c) and a part associated with resolved velocities (panel e) following Equation 10. Panels (d, f): Decomposition of the spatially redistributing advective term (panel b) into a part associated with the GM-parametrized eddy velocity (panel d) and a part associated with resolved velocities (panel f).

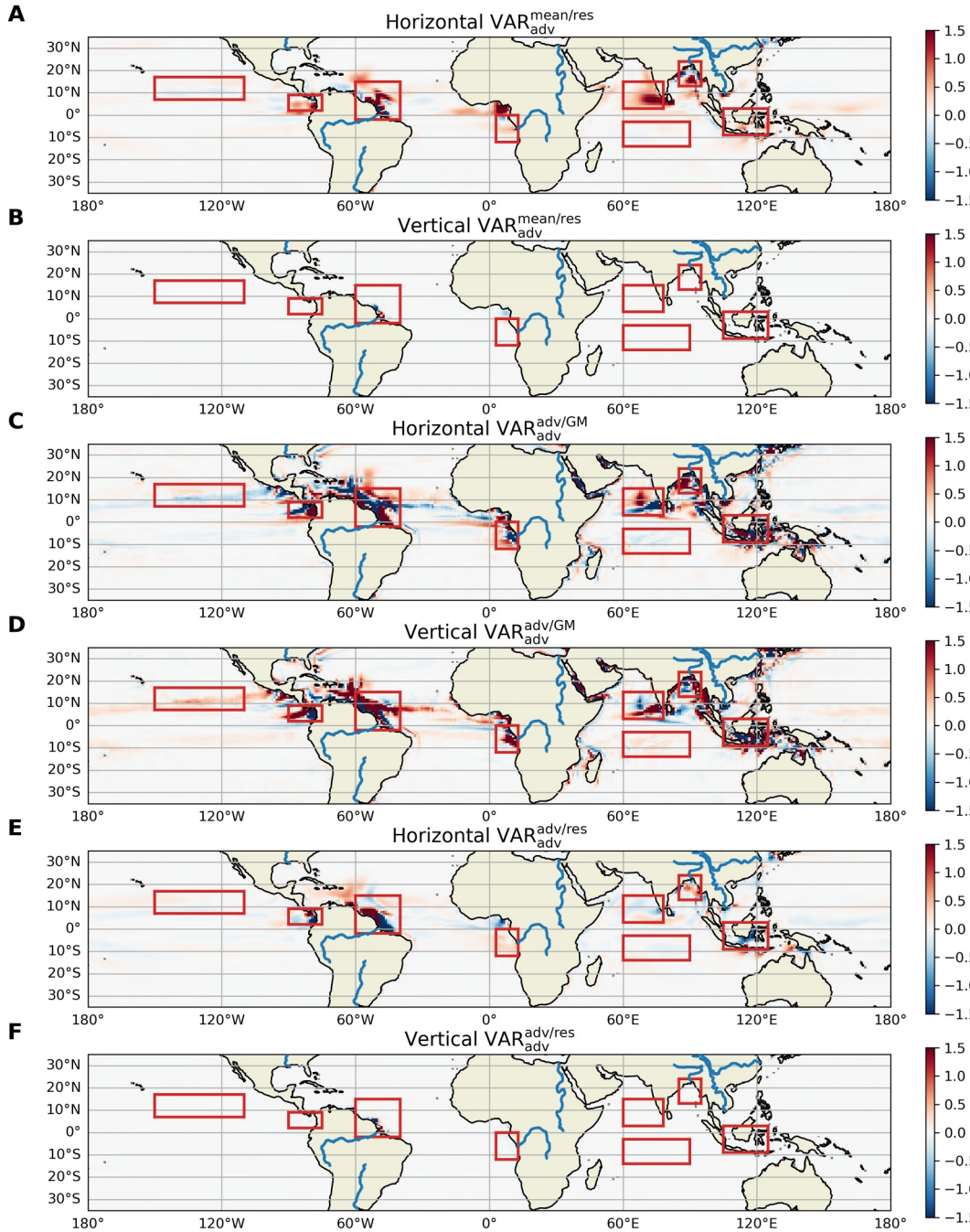

Figure 7. Horizontal (panels a, c, and e) and vertical (panels b, d, and f) decomposition of the three main advective terms (psu^2 yr^{-1}). Panels (a, b) represent the part of the salinity variance transfer term associated with resolved velocities, panels (c, d) the spatially redistributing term associated with parametrized velocities, and panels (e, f) the spatially redistributing term associated with resolved velocities.

time-averaged parameterized eddy velocity at the surface (Figure 8a). The surface intensity of the mean parameterized velocities depends mainly on the horizontal gradient of the time mean density field. River runoff creates an enhanced horizontal gradient of the time mean density field near the river mouths, which explains the importance of $VAR^{adv/GM}_{adv}$ in these regions. The part of $VAR^{adv/GM}_{adv}$ associated with anomalous seasonal velocities is generally weaker, except in some localized regions of the Panama Bight, the Amazon plume, and along the east coast of India (Figure 8c).

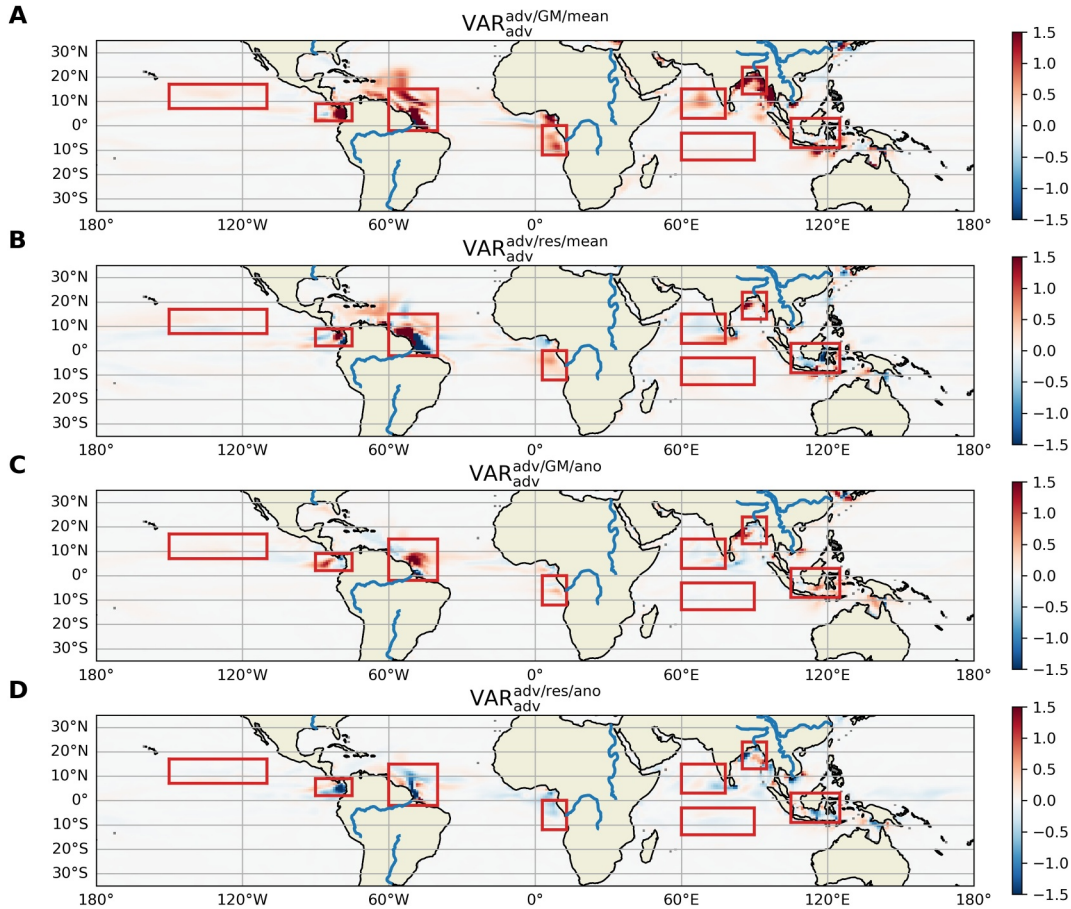

Figure 8. Decomposition of the advective spatially redistributing term into parts associated with the time-averaged velocity (Panels a and b) and parts associated with the anomalous seasonal velocities (Panels c and d) ($psu^2\ yr^{-1}$). Panels (a and c) represent the spatially redistributing term associated with parameterized velocities, and panels (b and d) represent the spatially redistributing term associated with resolved velocities.

Although the redistribution associated with the resolved component of the velocity (i.e., $VAR^{adv/res}_{adv}$) has a smaller amplitude than $VAR^{adv/GM}_{adv}$ (Figures 6d and f), this term can be locally important, especially in the Amazon plume region, where it is strongly negative (a sink) directly at the river mouth and positive (a source) north of the river mouth. Figure 7 panels E and F show that $VAR^{adv/res}_{adv}$ is associated with its horizontal part, and Figures 8b and 8d show that it is almost entirely due to the resolved mean horizontal velocities. It suggests that, in the Amazon plume region, the resolved horizontal mean circulation acts to transport the seasonal SSS variance to the northwest, along the Brazilian coast. This is consistent with the direction of the powerful North Brazil and Guiana currents, which flow northwestward along the coast (Johns et al., 1998).

4.5. Regional Average of the Local Variance Budgets in Selected Regions

To be more quantitative, we also provide in Figure 9 the spatial average of the main seasonal SSS variance budget terms in the eight regions outlined above and shown by the eight red boxes in previous figures. The main sink of SSS seasonal variance in seven of the eight regions under consideration is the term associated with vertical diffusion, representing at least 70% of the total sink in each regions. In contrast, the main sink in the eastern Arabian Sea region is associated with precipitation (88% of the total sink). In the Panama Bight, precipitation and the two advective terms are the three main sources, which are coherent with the results from Alory et al. (2012) who found an important role of precipitation and oceanic advection in setting the seasonal SSS variations in this region. The eastern Pacific and southern equatorial Indian regions follow similar dynamics, with the main source associated with the precipitation term and the main sink associated with vertical diffusion. Advective terms play

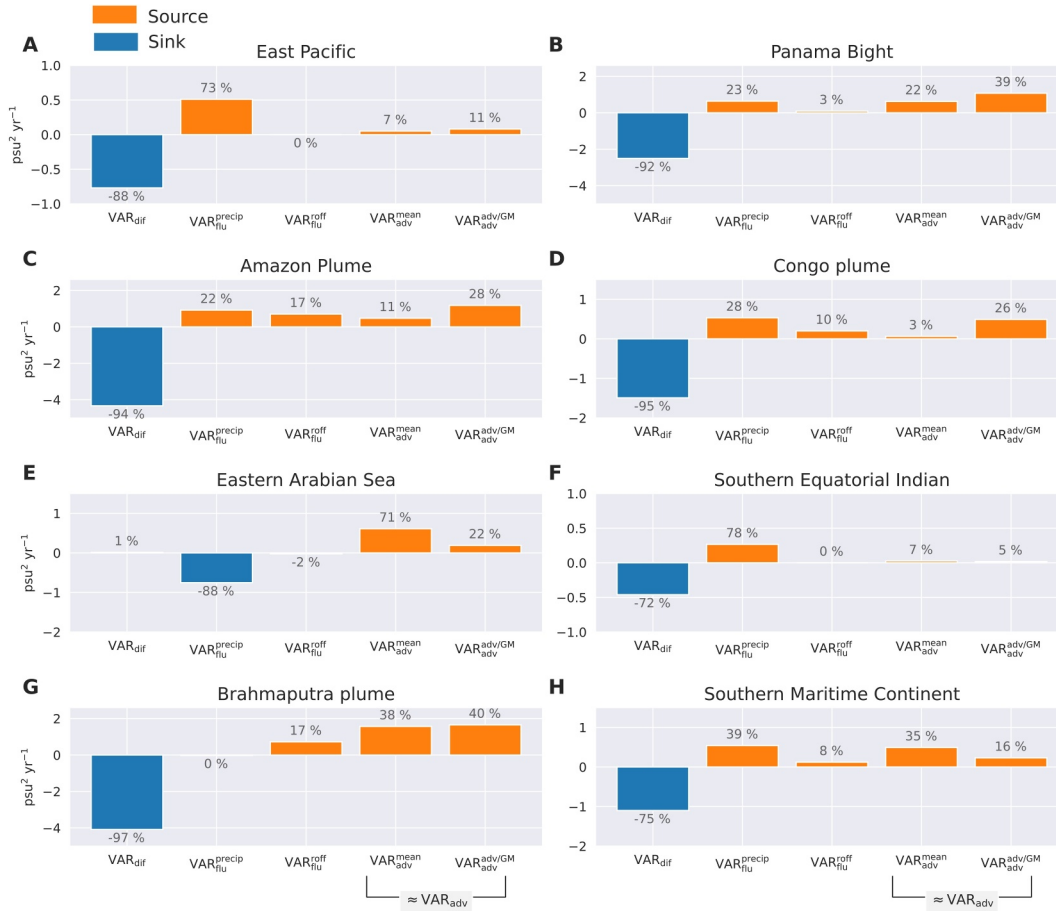

Figure 9. Spatial average of the main contributors to the seasonal SSS variance budget in the eight regions outlined by red boxes in Figures 1, 2, and 6: The East Pacific region (panel a), the Panama Bight region (panel b), the Amazon plume region (panel c), the Congo plume region (panel d), the eastern Arabian sea region (panel e), the Southern Equatorial Indian Ocean (panel f), the Brahmaputra plume region (panel g), and the southern Maritime Continent (panel h) ($psu^2\ yr^{-1}$). Sources are in orange while sinks are in blue. The contribution of each term in the total sink or total source is given as a percentage. VAR_{dif} represents the effect of the diffusive terms, VAR_{flu}^{precip} the effect of precipitation, VAR_{flu}^{roff} the effect of river runoff, VAR_{adv}^{mean} the oceanic advective term associated with the salinity flux across mean salinity surfaces (due to the anomalous residual velocities), and $VAR_{adv}^{adv/GM}$ the effect of the advective redistribution of seasonal SSS variance due to parametrized velocities. The sum of VAR_{adv}^{mean} and $VAR_{adv}^{adv/GM}$ is close to the total effect of the oceanic advective terms in these eight regions. Note that the sum of the source terms (sink terms) does not amount to 100% (−100%) because we only show the main contributors.

only a minor role in maintaining the variance of the SSS seasonal cycle in these two regions. In the Amazon plume region, the main sources of seasonal SSS variance are shared between precipitation, river runoff, and the redistribution of seasonal SSS variance by the parameterized eddy velocity $\left(VAR_{adv}^{adv/GM}\right)$. Although resolved velocities have been shown to play a significant role in redistributing the SSS variance in this region, this redistribution occurs within the selected box and therefore does not contribute significantly to its spatial average (see also Figure 6f). In the Congo plume region, the two main sources of seasonal SSS variance are the precipitation (28% of all sources) and the redistribution linked to parameterized eddy velocities (26%), while the term associated with river runoff only accounts for 10% of all sources. In the eastern Arabian Sea region, the main source of SSS variability is associated with the advective term (93% of all sources), which is the sum of the salinity variance transfer term due to the salinity flux in the direction opposite to the mean salinity gradient (71%) and of the spatially redistributing term due to the parameterized eddy velocities (22%). The average over this region indicates that diffusion plays no role in this selected region. However, it is apparent from Figure 2 that the diffusive term is a source in the eastern part of this region, thus acting to sustain the SSS seasonal cycle and a weak

sink in the western part. Thus, the sink and source effect in, respectively, the western and eastern parts of the region cancel out and give an overall zero effect of diffusion in the entire region. In the Ganges-Brahmaputra plume region (panel G), the main sources are associated with the spatially redistributing (40% of the total source) and salinity variance transfer terms (38%), and to the river runoff term, which also plays a significant role in sustaining the SSS variability (17%). In the southern Maritime Continent region (panel H), the sources of SSS variance are due to precipitation (39% of all sources), the two advective terms (35% and 16% of all sources), and a small contribution of river runoff (8%), while the main sink is due to vertical diffusion. These results are consistent with Lee et al. (2019) who showed that the seasonal cycle of SSS in this region is controlled by precipitation, river runoff, and ocean dynamics.

5. Conclusion

In this work, we have applied a new diagnostic called seasonal SVB to study the mechanisms of seasonal SSS variability in the tropical oceans. In the tropics, large amplitudes of seasonal SSS variability occur mainly in eight different regions: the eastern equatorial Pacific, the Panama Bight, the plume regions of the Amazon, Congo, Ganges-Brahmaputra rivers, the eastern Arabian Sea, the southern equatorial Indian, and the southern Maritime Continent region. Our results show that in these regions, the seasonal SSS variability is generally maintained by a combination of advective and freshwater flux terms, and balanced by vertical diffusion, which act to reduce the amplitude of the SSS variations. In all of the regions studied, with the exception of the eastern Arabian Sea, vertical diffusion always accounts for over 70% of all sinks. This effect of the vertical diffusion, found in our study, is in agreement with Camara et al. (2015) and Da-Allada et al. (2017) who outlined the important effect of vertical diffusion on the seasonal surface salinity variations in the tropical Atlantic, and with Akhil et al. (2014) for the Bay of Bengal.

We find that the freshwater flux term in the salinity variance equation is mainly due to the seasonal cycle of precipitation and the seasonal cycle of river runoff near the rivers' mouth. The evaporation effect in the control of the SSS seasonal cycle amplitude is negligible everywhere. We also show for the first time that in the eastern Arabian Sea as well as in some parts of the Bay of Bengal, precipitation acts as the main sink (88% of all sinks in the Arabian sea box) for seasonal SSS variations and is balanced by the effect of advection (93% of all sources in the Arabian sea box). A positive anomaly of precipitation is found over the region when the salinity is high (July–December) and a negative anomaly of precipitation when the salinity is low (January–June), which implies that precipitation damps the salinity variations. At the same time, changes in the circulations due to the reversing monsoon winds cause the advective term to increase the salinity anomaly when it is positive and to decrease it when it is negative implying that advection is a source term for the salinity variance. Because precipitation over these regions is mainly the result of the Indian monsoon and is not influenced by the SSS, the salinity/precipitation and salinity/advection relationships we find must be controlled by the effect of the monsoon on both oceanic circulation and precipitation. Previous studies based on mixed-layer salinity budget from observations (Akhil et al., 2023; Da-Allada et al., 2015; Rao & Sivakumar, 2003) have already shown that horizontal advection of freshwaters from the Bay of Bengal, driven by the seasonally reversing monsoon currents, as well as the vertical diffusion induced by the monsoon winds along the west Indian coast, play an important role in controlling the SSS seasonal cycle. In this study, we suggest for the first time that the effect of advection in this region is balanced by the effect of precipitation. The dynamics of the seasonal SSS variations are similar in the equatorial regions of the eastern Pacific and the southern Indian Ocean. The main source of the seasonal SSS variance in these two regions is associated with precipitation and the main sink with vertical diffusion. In these two regions, the advective term has a smaller amplitude than that of the precipitation and diffusion terms and is almost in quadrature with the salinity variations, explaining its weak contribution to the SSS variance budget. In the Bight of Panama and the southern Maritime Continent, the dynamics controlling the seasonal SSS amplitude are more complex than in the two previous regions, because several terms act as sources: precipitation and the two different advective terms, that is, the transfer and the spatial redistribution of the seasonal SSS variance.

One of the main advantages of our diagnostic is that it allows to rigorously decompose the effect of oceanic advection into several terms with a clear physical interpretation. We show that the oceanic advective term is mainly the sum of two terms—first, a term associated with the spatial redistribution of the salinity variance by the ocean circulation, which would disappear if integrated over the whole ocean volume, and second, a term due to the salinity variance transfer between the time mean ($\frac{\overline{S}^2}{2}$ reservoir) and seasonal circulation ($\frac{\overline{(S')^2}}{2}$ reservoir). The

salinity variance transfer term can be seen as the result of the codependence of the time-averaged salinity field and the seasonal anomalies. This term is associated with the salinity flux in the direction of the mean salinity gradient, which would not disappear if integrated over the global ocean. If the effect associated with the first term of the decomposition, that is, the redistribution of salinity variance by the circulation, is relatively well known, the effect of the second term has, to the best of our knowledge, never been described before in the context of SSS seasonal variations.

We have shown that the spatial redistribution term is mainly driven by the parameterized eddy-induced time mean velocities in almost all regions and acts as a local source of SSS seasonal variance. Previous studies of the tropical SSS seasonal cycle have only decomposed the advective term into horizontal and vertical components and/or study the impact of geostrophic or Ekman balance (Akhil et al., 2014; Camara et al., 2015; Da-Allada et al., 2013, 2014). In this work, we have shown for the first time that an important part of this advective term is associated to the (parameterized) eddy-induced velocities, due to both horizontal and vertical components. This is coherent with several studies reporting the presence of eddies in the regions considered in this study (Aguedjou et al., 2019; Hareesh Kumar et al., 2013; Schütte et al., 2016; Trott et al., 2019). Additionally, although the advective term associated with the mean resolved velocities is in almost all regions smaller than the one linked with the parameterized eddy-induced velocities, it is locally important in the Amazon river plume region. In this region, it is indeed found that the horizontal part of the mean resolved velocities is almost entirely due to its time-averaged horizontal component and that its patterns are coherent in this region with a northwestward advection of variance caused by the North Brazil Current.

The second term of the decomposition, associated with the seasonal SSS variance transfer, is found to be an important source of seasonal SSS variance in most of the regions considered. For instance, it is the main source of seasonal SSS variance in the eastern Arabian Sea, representing 71% of all sources of this region. In all regions, it is associated with the horizontal salinity flux in the direction of the horizontal gradient of the time mean salinity and, unlike the spatial redistribution term, is mostly due to resolved velocities. Because it disappears when considering the sum of the mean and anomalous circulation (see Appendix B), this term can be thought as a redistribution of salinity variance in the temporal space, that is, between the time mean circulation and the seasonal circulation.

The main limitation of this study is related to the spatial resolution of ECCO v4, which is about 111 km at low latitudes and thus cannot explicitly resolve the mesoscale eddy variability. Because we find that parameterized eddy-induced transports are important components of the SSS seasonal cycle balance, it may be expected that important differences would arise in a model with sufficient spatial resolution to resolve the eddy field. Indeed, studies suggest that eddies play an important role in the dynamics of tropical river plume regions (e.g., Olivier et al., 2024). However, the comparison between the ECCO SSS seasonal cycle and satellite observations shows that ECCO v4 is able to correctly reproduce the main features of the SSS variations, suggesting that the mesoscale parameterization captures the main effect of the mesoscale on the SSS seasonal field. Although the overall agreement between the seasonal SSS variance found in ECCO and observations is good, seasonal SSS variance appears to be underestimated in several river plumes such as the Mississippi and the Amazon river plume (Figure 1); we hypothesize that this is a consequence of the coarse resolution of ECCO v4. Future studies should consider repeating the same analysis presented here using an eddy-resolving model in order to (a) improve the representation of seasonal SSS variability, (b) assess the effect of mesoscale eddies on the SSS variability and SSS variance budget when explicitly resolved, and (c) assess the parametrization of the mesoscale eddies, which is also used in current CMIP6 climate models. Finally, the results presented in this article may depend in part on the representation of the ocean state given by ECCO v4, either due to errors in the model representation, uncertainties in the assimilated observations, or other factors. Future work should therefore also consider assessing uncertainties in the salinity variance budget, either by repeating the same diagnostic in different numerical models and observations, and/or by applying the diagnostic to ad hoc sensitivity experiments recently developed for estimating uncertainties within ECCO v4 (see Wei et al., preprint).

Appendix A: Interpretation of $\overline{\frac{1}{2}\frac{\partial (S')^2}{\partial t}}$

Let us call $S_a = SSS - \overline{SSS}$ the 23-year monthly time series of SSS anomalies at a given location, with $\overline{SSS}$ the time mean. If we assume that the amplitude of the seasonal salinity cycle increases over the studied period of $T = 23$ years, then we should have that $\overline{\frac{\partial (S_a)^2}{\partial t}} = (S_a)^2(t = T) - (S_a)^2(t = 0) > 0$. Then, because

$\frac{1}{2}\frac{\partial S_a^2}{\partial t} = S_a\frac{\partial S_a}{\partial t}$, we also have that $\overline{S_a\frac{\partial S_a}{\partial t}} > 0$, which means that S_a and $\frac{\partial S_a}{\partial t}$ are not in quadrature. In this article, we follow the common practice of calculating the mean seasonal cycle by averaging the monthly salinity anomalies time series over the studied period, resulting in a time series of 12 values (see also Equation 2), one point for each calendar month. This methodology is applied to S_a and to $\frac{\partial S_a}{\partial t}$ and results in $S' = (S_a)'$ and $\frac{\partial S'}{\partial t} = \left(\frac{\partial S_a}{\partial t}\right)'$, respectively, the mean seasonal cycle of S_a and $\frac{\partial S_a}{\partial t}$ where $(X)'$ represents the mean seasonal cycle of X. S' captures the mean phase of the seasonal cycle of S_a and $\frac{\partial S'}{\partial t}$ the mean phase of the seasonal cycle of $\frac{\partial S_a}{\partial t}$; it follows that if the product $\overline{S_a\frac{\partial S_a}{\partial t}}$ is nonzero because the seasonal cycle amplitude increases, then $\overline{S'\frac{\partial S'}{\partial t}}$ will also be nonzero and will reflect the mean seasonal increase of the amplitude over the studied period.

Appendix B: Role of Advection on SSS Variance

In this appendix, we show that the role of advection, when salinity is not separated into mean and anomaly, is only to redistribute spatially the total squared salinity S^2. The salinity variance transfer term (i.e., $\mathrm{VAR}_{\mathrm{adv}}^{\mathrm{mean}} = -\overline{\mathbf{V}'S'}\cdot\nabla\overline{S}$) only appears when the salinity is decomposed into time mean and anomaly. To keep the demonstration simple, we consider only the advective terms and assume that the circulation is only made of two components: the mean circulation and the seasonal cycle anomaly so that $S = \overline{S} + S'$ and $\mathbf{V} = \overline{\mathbf{V}} + \mathbf{V}'$. First, an equation for the squared salinity is as follows:

$$\frac{1}{2}\frac{\partial S^2}{\partial t} = -\nabla\cdot\mathbf{V}\frac{S^2}{2} \tag{B1}$$

Because the right-hand side is a divergence of a flux, this term would disappear if we integrated it over the ocean volume, and it shows that the circulation only acts to redistribute S^2. Moreover, decomposing this equation into its time average and anomalous components yields the following:

$$\frac{1}{2}\frac{\partial S^2}{\partial t} = \frac{1}{2}\frac{\partial \overline{S}^2}{\partial t} + \frac{1}{2}\frac{\partial (S')^2}{\partial t} + \frac{\partial \overline{S}S'}{\partial t} = -\nabla\cdot\mathbf{V}\frac{\overline{S}^2}{2} - \nabla\cdot\mathbf{V}\frac{(S')^2}{2} - \nabla\cdot\mathbf{V}\overline{S}S' \tag{B2}$$

which gives the following when time-averaged:

$$\frac{1}{2}\overline{\frac{\partial S^2}{\partial t}} = \frac{1}{2}\frac{\partial \overline{S}^2}{\partial t} + \frac{1}{2}\overline{\frac{\partial (S')^2}{\partial t}} = -\nabla\cdot\overline{\mathbf{V}}\frac{\overline{S}^2}{2} - \nabla\cdot\mathbf{V}\overline{\frac{(S')^2}{2}} - \nabla\cdot\overline{S}\,\overline{\mathbf{V}'S'} \tag{B3}$$

that is, we recover the sum of Equations 9 and 7, $\mathrm{VAR}_{\mathrm{adv}}^{\mathrm{mean}}$, only appears when considering the budgets for $\overline{S}^2$ and S'^2 separately as shown by Equations 9 and 7.

Acknowledgments
ECCO v4r4 salinity budget computations were greatly facilitated by the existence of the *ecco_v4_py* Python library, and by several tutorials, which can be found at https://ecco-v4-python-tutorial.readthedocs.io/. AH is supported by an ESA living planet fellowship under the PACIFIC project and by the VACARM project funded through the French CNRS/INSU/LEFE program. ST is supported by a UBO-CNES PhD fellowship. WL is supported by the EERIE project (Grant Agreement No 101081383) funded by the European Union. This work is a contribution to the IMHOTEP project funded by CNES through the Ocean Surface Topography Science Team (OSTST). We also thank two anonymous reviewers whose comments helped to significantly improve an earlier version of the manuscript.

Data Availability Statement

This study uses ECCO v4r4, which can be found here: https://ecco-group.org/products-ECCO-V4r4.htm. The CCI SSS data set can be found on the ceda website: https://catalogue.ceda.ac.uk.

References

Aguedjou, H. M. A., Dadou, I., Chaigneau, A., Morel, Y., & Alory, G. (2019). Eddies in the tropical Atlantic Ocean and their seasonal variability. *Geophysical Research Letters*, *46*(21), 12156–12164. https://doi.org/10.1029/2019GL083925

Akhil, V. P., Durand, F., Lengaigne, M., Vialard, J., Keerthi, M. G., Gopalakrishna, V. V., et al. (2014). A modeling study of the processes of surface salinity seasonal cycle in the Bay of Bengal. *Journal of Geophysical Research: Oceans*, *119*(6), 3926–3947. https://doi.org/10.1002/2013JC009632

Akhil, V. P., Lengaigne, M., Krishnamohan, K. S., Keerthi, M. G., & Vialard, J. (2023). Southeastern Arabian Sea salinity variability: Mechanisms and influence on surface temperature. *Climate Dynamics*, *61*(7–8), 3737–3754. https://doi.org/10.1007/s00382-023-06765-z

Alory, G., Maes, C., Delcroix, T., Reul, N., & Illig, S. (2012). Seasonal dynamics of sea surface salinity off Panama: The far eastern pacific fresh pool. *Journal of Geophysical Research*, *117*(C4). https://doi.org/10.1029/2011JC007802

Arzel, O., Huck, T., & Colin de Verdière, A. (2006). The different nature of the interdecadal variability of the thermohaline circulation under mixed and flux boundary conditions. *Journal of Physical Oceanography*, *36*(9), 1703–1718. https://doi.org/10.1175/jpo2938.1

Arzel, O., Huck, T., & Colin de Verdière, A. (2018). The internal generation of the Atlantic Ocean interdecadal variability. *Journal of Climate*, *31*(16), 6411–6432. https://doi.org/10.1175/JCLI-D-17-0884.1

Boucharel, J., Timmermann, A., Santoso, A., England, M. H., Jin, F.-F., & Balmaseda, M. A. (2015). A surface layer variance heat budget for ENSO. *Geophysical Research Letters*, *42*(9), 3529–3537. https://doi.org/10.1002/2015GL063843

Boutin, J., Reul, N., Koehler, J., Martin, A., Catany, R., Guimbard, S., et al. (2021). Satellite-based sea surface salinity designed for ocean and climate studies. *Journal of Geophysical Research: Oceans*, *126*(11), e2021JC017676. https://doi.org/10.1029/2021JC017676

Boyer, T. P., Levitus, S., Antonov, J. I., Locarnini, R. A., & Garcia, H. E. (2005). Linear trends in salinity for the World Ocean, 1955–1998. *Geophysical Research Letters*, *32*(1), 2004GL021791. https://doi.org/10.1029/2004GL021791

Buckley, M. W., Ferreira, D., Campin, J.-M., Marshall, J., & Tulloch, R. (2012). On the relationship between decadal buoyancy anomalies and variability of the Atlantic meridional overturning circulation. *Journal of Climate*, *25*(23), 8009–8030. https://doi.org/10.1175/JCLI-D-11-00505.1

Camara, I., Kolodziejczyk, N., Mignot, J., Lazar, A., & Gaye, A. T. (2015). On the seasonal variations of salinity of the tropical Atlantic mixed layer. *Journal of Geophysical Research: Oceans*, *120*(6), 4441–4462. https://doi.org/10.1002/2015JC010865

Colin de Verdière, A., & Huck, T. (1999). Baroclinic instability: An oceanic wavemaker for interdecadal variability. *Journal of Physical Oceanography*, *29*(5), 893–910. https://doi.org/10.1175/1520-0485(1999)029<0893:biaowf>2.0.co;2

Curry, R., Dickson, B., & Yashayaev, I. (2003). A change in the freshwater balance of the Atlantic Ocean over the past four decades. *Nature*, *426*(6968), 826–829. https://doi.org/10.1038/nature02206

Da-Allada, C. Y., Alory, G., Du Penhoat, Y., Kestenare, E., Durand, F., & Hounkonnou, N. M. (2013). Seasonal mixed-layer salinity balance in the tropical Atlantic Ocean: Mean state and seasonal cycle. *Journal of Geophysical Research: Oceans*, *118*(1), 332–345. https://doi.org/10.1029/2012JC008357

Da-Allada, C. Y., du Penhoat, Y., Jouanno, J., Alory, G., & Hounkonnou, N. M. (2014). Modeled mixed-layer salinity balance in the Gulf of Guinea: Seasonal and interannual variability. *Ocean Dynamics*, *64*(12), 1783–1802. https://doi.org/10.1007/s10236-014-0775-9

Da-Allada, C. Y., Gaillard, F., & Kolodziejczyk, N. (2015). Mixed-layer salinity budget in the tropical Indian Ocean: Seasonal cycle based only on observations. *Ocean Dynamics*, *65*(6), 845–857. https://doi.org/10.1007/s10236-015-0837-7

Da-Allada, C. Y., Jouanno, J., Gaillard, F., Kolodziejczyk, N., Maes, C., Reul, N., & Bourlès, B. (2017). Importance of the equatorial undercurrent on the sea surface salinity in the Eastern Equatorial Atlantic in boreal spring. *Journal of Geophysical Research: Oceans*, *122*(1), 521–538. https://doi.org/10.1002/2016JC012342

Delcroix, T., & Hénin, C. (1991). Seasonal and interannual variations of sea surface salinity in the tropical Pacific Ocean. *Journal of Geophysical Research*, *96*(C12), 22135–22150. https://doi.org/10.1029/91JC02124

Delcroix, T., Henin, C., Porte, V., & Arkin, P. (1996). Precipitation and sea-surface salinity in the tropical Pacific Ocean. *Deep Sea Research Part I: Oceanographic Research Papers*, *43*(7), 1123–1141. https://doi.org/10.1016/0967-0637(96)00048-9

Dessier, A., & Donguy, J. R. (1994). The sea surface salinity in the tropical Atlantic between 10°S and 30°N—Seasonal and interannual variations (1977–1989). *Deep Sea Research Part I: Oceanographic Research Papers*, *41*(1), 81–100. https://doi.org/10.1016/0967-0637(94)90027-2

Durack, P. J., Wijffels, S. E., & Matear, R. J. (2012). Ocean salinities reveal strong global water cycle intensification during 1950 to 2000. *Science*, *336*(6080), 455–458. https://doi.org/10.1126/science.1212222

Fathrio, I., Manda, A., Iizuka, S., Kodama, Y.-M., & Ishida, S. (2017). Evaluation of CMIP5 models on sea surface salinity in the Indian Ocean. *IOP Conference Series: Earth and Environmental Science* (Vol. 54(1), 012039). https://doi.org/10.1088/1755-1315/54/1/012039

Fekete, B. M., Vörösmarty, C. J., & Grabs, W. (2002). High-resolution fields of global runoff combining observed river discharge and simulated water balances. *Global Biogeochemical Cycles*, *16*(3), 15–21. https://doi.org/10.1029/1999gb001254

Forget, G., Campin, J.-M., Heimbach, P., Hill, C. N., Ponte, R. M., & Wunsch, C. (2015). ECCO version 4: An integrated framework for non-linear inverse modeling and global ocean state estimation. *Geoscientific Model Development*, *8*(10), 3071–3104. https://doi.org/10.5194/gmd-8-3071-2015

Gastineau, G., Mignot, J., Arzel, O., & Huck, T. (2018). North Atlantic Ocean internal decadal variability: Role of the mean state and Ocean-atmosphere coupling. *Journal of Geophysical Research: Oceans*, *123*(8), 5949–5970. https://doi.org/10.1029/2018JC014074

Gent, P. R., & Mcwilliams, J. C. (1990). Isopycnal mixing in ocean circulation models. *Journal of Physical Oceanography*, *20*(1), 150–155. https://doi.org/10.1175/1520-0485(1990)020<0150:imiocm>2.0.co;2

Gregg, M., D'Asaro, E., Riley, J., & Kunze, E. (2018). Mixing efficiency in the Ocean. *Annual Review of Marine Science*, *10*(1), 443–473. https://doi.org/10.1146/annurev-marine-121916-063643

Guan, C., & McPhaden, M. J. (2016). Ocean processes affecting the twenty-first-century shift in ENSO SST variability. *Journal of Climate*, *29*(19), 6861–6879. https://doi.org/10.1175/JCLI-D-15-0870.1

Guan, C., McPhaden, M. J., Wang, F., & Hu, S. (2019). Quantifying the role of oceanic feedbacks on ENSO asymmetry. *Geophysical Research Letters*, *46*(4), 2140–2148. https://doi.org/10.1029/2018GL081332

Guimbard, S., Reul, N., Chapron, B., Umbert, M., & Maes, C. (2017). Seasonal and interannual variability of the eastern tropical Pacific fresh pool. *Journal of Geophysical Research: Oceans*, *122*(3), 1749–1771. https://doi.org/10.1002/2016JC012130

Gulev, S., Thorne, P., Ahn, J., Dentener, F., Domingues, C., Gerland, S., et al. (2021). Changing state of the climate system [Book Section]. In V. Masson-Delmotte (Ed.), *Climate change 2021: The physical science basis. contribution of working group i to the sixth assessment report of the intergovernmental panel on climate change (chap. 2)*. Cambridge University Press. https://doi.org/10.1017/9781009157896.004

Hareesh Kumar, P. V., Mathew, B., Ramesh Kumar, M. R., Raghunadha Rao, A., Jagadeesh, P. S. V., Radhakrishnan, K. G., & Shyni, T. N. (2013). Thermohaline front'off the east coast of India and its generating mechanism. *Ocean Dynamics*, *63*(11), 1175–1180. https://doi.org/10.1007/s10236-013-0652-y

Heimbach, P., Hill, C., & Giering, R. (2005). An efficient exact adjoint of the parallel MIT General Circulation Model, generated via automatic differentiation. *Future Generation Computer Systems*, *21*(8), 1356–1371. https://doi.org/10.1016/j.future.2004.11.010

Held, I. M., & Soden, B. J. (2006). Robust responses of the hydrological cycle to global warming. *Journal of Climate*, *19*(21), 5686–5699. https://doi.org/10.1175/jcli3990.1

Hochet, A., Huck, T., Arzel, O., Sévellec, F., Colin de Verdière, A., Mazloff, M., & Cornuelle, B. (2020). Direct temporal cascade of temperature variance in eddy-permitting simulations of multidecadal variability. *Journal of Climate*, *33*(21), 9409–9425. https://doi.org/10.1175/JCLI-D-19-0921.1

Hochet, A., Huck, T., Arzel, O., Sévellec, F., & de Verdière, A. C. (2022). Energy transfers between multidecadal and turbulent variability. *Journal of Climate*, *35*(4), 1157–1178. https://doi.org/10.1175/JCLI-D-21-0136.1

Hochet, A., Huck, T., & Colin de Verdière, A. (2015). Large-scale baroclinic instability of the mean oceanic circulation: A local approach. *Journal of Physical Oceanography*, *45*(11), 2738–2754. https://doi.org/10.1175/JPO-D-15-0084.1

Hochet, A., Lique, C., Sevellec, F., & Llovel, W. (2024). Drivers of interannual salinity variability in the Arctic Ocean. *Journal of Geophysical Research: Oceans*, *129*(6), e2023JC020852. https://doi.org/10.1029/2023JC020852

Hochet, A., Llovel, W., Huck, T., & Sevellec, F. (2024). Advection surface-flux balance controls the seasonal steric sea level amplitude. *Scientific Reports*, *14*(1), 10644. https://doi.org/10.1038/s41598-024-61447-y

Hochet, A., Llovel, W., Sévellec, F., & Huck, T. (2023). Sources and sinks of interannual steric sea level variability. *Journal of Geophysical Research: Oceans*, *128*(4), e2022JC019335. https://doi.org/10.1029/2022jc019335

Houndegnonto, O. J., Kolodziejczyk, N., Maes, C., Bourlès, B., Da-Allada, C. Y., & Reul, N. (2021). Seasonal variability of freshwater plumes in the eastern gulf of Guinea as inferred from satellite measurements. *Journal of Geophysical Research: Oceans*, *126*(5), e2020JC017041. https://doi.org/10.1029/2020JC017041

Johns, W. E., Lee, T. N., Beardsley, R. C., Candela, J., Limeburner, R., & Castro, B. (1998). Annual cycle and variability of the North Brazil current. *Journal of Physical Oceanography*, *28*(1), 103–128. https://doi.org/10.1175/1520-0485(1998)028⟨0103:ACAVOT⟩2.0.CO;2

Lee, T., Fournier, S., Gordon, A. L., & Sprintall, J. (2019). Maritime Continent water cycle regulates low-latitude chokepoint of global ocean circulation. *Nature Communications*, *10*(1), 2103. https://doi.org/10.1038/s41467-019-10109-z

Liu, B., Gan, B., Jia, F., & Wu, L. (2024). Impact of the North Pacific meridional mode on the tropical Pacific modulated by the interdecadal Pacific Oscillation. *Journal of Climate*, *37*(7), 2199–2216. https://doi.org/10.1175/JCLI-D-23-0448.1

Liu, Y., Cheng, L., Pan, Y., Tan, Z., Abraham, J., Zhang, B., et al. (2022). How well do CMIP6 and CMIP5 models simulate the climatological seasonal variations in ocean salinity? *Advances in Atmospheric Sciences*, *39*(10), 1650–1672. https://doi.org/10.1007/s00376-022-1381-2

Lukas, R., & Lindstrom, E. (1991). The mixed layer of the western equatorial Pacific Ocean. *Journal of Geophysical Research*, *96*(S01), 3343–3357. https://doi.org/10.1029/90jc01951

MacCready, P., Geyer, W. R., & Burchard, H. (2018). Estuarine exchange flow is related to mixing through the salinity variance budget. *Journal of Physical Oceanography*, *48*(6), 1375–1384. https://doi.org/10.1175/jpo-d-17-0266.1

Matias, A., Tanajura, C., Pereira, J., & Costa, F. (2024). Seasonal variation of the sea surface salinity in the Western tropical North Atlantic on two contrasting years of precipitation in the Amazon Basin. *Ocean Dynamics*, *74*(4), 269–285. https://doi.org/10.1007/s10236-024-01602-1

Mignot, J., Lazar, A., & Lacarra, M. (2012). On the formation of barrier layers and associated vertical temperature inversions: A focus on the northwestern tropical Atlantic. *Journal of Geophysical Research*, *117*(C2). https://doi.org/10.1029/2011JC007435

Olivier, L., Reverdin, G., Boutin, J., Laxenaire, R., Iudicone, D., Pesant, S., et al. (2024). Late summer northwestward amazon plume pathway under the action of the North Brazil current rings. *Remote Sensing of Environment*, *307*, 114165. https://doi.org/10.1016/j.rse.2024.114165

Osborn, T. R., & Cox, C. S. (1972). Oceanic fine structure. *Geophysical Fluid Dynamics*, *3*(4), 321–345. https://doi.org/10.1080/03091927208236085

Qu, T., Gao, S., & Fukumori, I. (2011). What governs the North Atlantic salinity maximum in a global GCM? *Geophysical Research Letters*, *38*(7). https://doi.org/10.1029/2011GL046757

Rao, R. R., & Sivakumar, R. (2003). Seasonal variability of sea surface salinity and salt budget of the mixed layer of the North Indian Ocean. *Journal of Geophysical Research*, *108*(C1), 9–1. https://doi.org/10.1029/2001JC000907

Reul, N., Grodsky, S., Arias, M., Boutin, J., Catany, R., Chapron, B., et al. (2020). Sea surface salinity estimates from spaceborne l-band radiometers: An overview of the first decade of observation (2010–2019). *Remote Sensing of Environment*, *242*, 111769. https://doi.org/10.1016/j.rse.2020.111769

Reverdin, G., Kestenare, E., Frankignoul, C., & Delcroix, T. (2007). Surface salinity in the Atlantic Ocean (30°S–50°N). *Progress in Oceanography*, *73*(3), 311–340. https://doi.org/10.1016/j.pocean.2006.11.004

Schmitt, R. W. (1995). The ocean component of the global water cycle. *Reviews of Geophysics*, *33*(S2), 1395–1409. https://doi.org/10.1029/95RG00184

Schütte, F., Brandt, P., & Karstensen, J. (2016). Occurrence and characteristics of mesoscale eddies in the tropical Northeastern Atlantic Ocean. *Ocean Science*, *12*(3), 663–685. https://doi.org/10.5194/os-12-663-2016

Shankar, D., Vinayachandran, P. N., & Unnikrishnan, A. S. (2002). The monsoon currents in the North Indian Ocean. *Progress in Oceanography*, *52*(1), 63–120. https://doi.org/10.1016/S0079-6611(02)00024-1

Skliris, N., Marsh, R., Josey, S. A., Good, S. A., Liu, C., & Allan, R. P. (2014). Salinity changes in the World Ocean since 1950 in relation to changing surface freshwater fluxes. *Climate Dynamics*, *43*(3–4), 709–736. https://doi.org/10.1007/s00382-014-2131-7

Terray, L., Corre, L., Cravatte, S., Delcroix, T., Reverdin, G., & Ribes, A. (2012). Near-surface salinity as nature's rain gauge to detect human influence on the tropical water cycle. *Journal of Climate*, *25*(3), 958–977. https://doi.org/10.1175/JCLI-D-10-05025.1

Thakur, R., Shroyer, E. L., Govindarajan, R., Farrar, J. T., Weller, R. A., & Moum, J. N. (2019). Seasonality and buoyancy suppression of turbulence in the Bay of Bengal. *Geophysical Research Letters*, *46*(8), 4346–4355. https://doi.org/10.1029/2018GL081577

Trott, C. B., Subrahmanyam, B., Chaigneau, A., & Roman-Stork, H. L. (2019). Eddy-induced temperature and salinity variability in the Arabian Sea. *Geophysical Research Letters*, *46*(5), 2734–2742. https://doi.org/10.1029/2018GL081605

Tzortzi, E., Josey, S. A., Srokosz, M., & Gommenginger, C. (2013). Tropical Atlantic salinity variability: New insights from SMOS. *Geophysical Research Letters*, *40*(10), 2143–2147. https://doi.org/10.1002/grl.50225

Vinogradova, N. T., & Ponte, R. M. (2013). Clarifying the link between surface salinity and freshwater fluxes on monthly to interannual time scales. *Journal of Geophysical Research: Oceans*, *118*(6), 3190–3201. https://doi.org/10.1002/jgrc.20200

Wei, Y., Pillar, H., Heimbach, P., Nguyen, A. T., Forget, G., Wang, O., et al. (preprint). An assessment of uncertainty in the ECCO global ocean-sea ice state estimate due to atmospheric forcing uncertainty. *ESS Open Archive*. https://doi.org/10.22541/essoar.173343662.26300741/v1

Yu, L. (2011). A global relationship between the ocean water cycle and near-surface salinity. *Journal of Geophysical Research*, *116*(C10), C10025. https://doi.org/10.1029/2010JC006937

Yu, L. (2014). Coherent evidence from Aquarius and Argo for the existence of a shallow low-salinity convergence zone beneath the Pacific Itcz. *Journal of Geophysical Research: Oceans*, *119*(11), 7625–7644. https://doi.org/10.1002/2014JC010030

Yu, L. (2023). Connecting subtropical salinity maxima to tropical salinity minima: Synchronization between ocean dynamics and the water cycle. *Progress in Oceanography*, *219*, 103172. https://doi.org/10.1016/j.pocean.2023.103172

Yu, L., Josey, S. A., Bingham, F. M., & Lee, T. (2020). Intensification of the global water cycle and evidence from Ocean Salinity: A synthesis review. *Annals of the New York Academy of Sciences*, *1472*(1), 76–94. https://doi.org/10.1111/nyas.14354

Zika, J. D., Skliris, N., Nurser, A. J. G., Josey, S. A., Mudryk, L., Laliberté, F., & Marsh, R. (2015). Maintenance and broadening of the Ocean's salinity distribution by the water cycle. *Journal of Climate*, *28*(24), 9550–9560. https://doi.org/10.1175/JCLI-D-15-0273.1